

# The Isotopic Links from Planet Forming Regions to the Solar System

H. Nomura<sup>1,2</sup>, K. Furuya<sup>1</sup>, M.A. Cordiner<sup>3,4</sup>, S.B. Charnley<sup>3</sup>, C.M.O'D. Alexander<sup>5</sup>, C.A. Nixon<sup>3</sup>, V.V. Guzman<sup>6</sup>, H. Yurimoto<sup>7</sup>, T. Tsukagoshi<sup>1</sup>, T. Iino<sup>8</sup>

<sup>1</sup> Division of Science, National Astronomical Observatory of Japan, 2-21-1 Osawa, Mitaka, Tokyo 181-8588, Japan

<sup>2</sup> The Graduate University for Advanced Studies, SOKENDAI, 2-21-1 Osawa, Mitaka, Tokyo 181-8588, Japan

<sup>3</sup> Solar System Exploration Division, NASA Goddard Space Flight Center, Greenbelt, MD, USA

<sup>4</sup> Department of Physics, Catholic University of America, Washington DC, USA

<sup>5</sup> Earth and Planets Laboratory, Carnegie Institution of Washington, 5241 Broad Branch Road NW, Washington, DC 20015, USA

<sup>6</sup> Instituto de Astrofísica, Pontificia Universidad Católica de Chile, Av. Vicuña Mackenna 4860, 7820436 Macul, Santiago, Chile

<sup>7</sup> Department of Natural History Sciences, Hokkaido University, Sapporo, Hokkaido 060-0810, Japan

<sup>8</sup> Information Technology Center, The University of Tokyo, 2-11-16, Yayoi, Bunkyo, Tokyo 113-8658, Japan

Isotopic ratios provide a powerful tool for understanding the origins of materials, including the volatile and refractory matter within solar system bodies. Recent high sensitivity observations of molecular isotopologues, in particular with ALMA, have brought us new information on isotopic ratios of hydrogen, carbon, nitrogen and oxygen in star and planet forming regions as well as the solar system objects. Solar system exploration missions, such as Rosetta and Cassini, have given us further new insights. Meanwhile, the recent development of sophisticated models for isotope chemistry including detailed gas-phase and grain surface reaction network has made it possible to discuss how isotope fractionation in star and planet forming regions is imprinted into the icy mantles of dust grains, preserving a record of the initial isotopic state of solar system materials. This chapter reviews recent progress in observations of molecular isotopologues in extra-solar planet forming regions, prestellar/protostellar cores and protoplanetary disks, as well as objects in our solar system — comets, meteorites, and planetary/satellite atmospheres — and discusses their connection by means of isotope chemical models.

## 1. INTRODUCTION

### 1.1. Solar system formation and isotope fractionation

Isotopic ratios are used in various fields of research to trace the chemical evolution of different materials. They are valuable not only for studying the origins of objects in our solar system, but also for investigating chemical pathways in the terrestrial environment, biosphere, and living organisms. For relatively complex molecules, position-specific isotope analysis has been established as one of the useful methods to analyse the origin of materials, such as biosynthetic pathways. Isotope analysis of functional groups in organic material in meteorites has been a highly beneficial tool for understanding their structure and origin (e.g., Glavin *et al.* 2018). Even in the case of astronomical observations, anomalies of the  $^{12}\text{C}/^{13}\text{C}$  ratio at different positions of carbon-chain molecules have been found in molecular clouds (e.g., Takano *et al.* 1998; Sakai *et al.* 2010; Giesen *et al.* 2020).

The formation of the solar system must be considered in the context of the formation of low-mass stars and their surrounding planetary systems (e.g., Hayashi *et al.* 1985; Pineda *et al.* 2022; Tsukamoto *et al.* 2022; Drazkowska *et al.* 2022). The composition of gas giant planets will be similar to that of nebula gas, while rocky/ice planets and small bodies reflect the composition of refractory material

and ice in/on the dust grains from which they accreted. Inside solar system objects, isotopic fractionations are further enhanced/diminished by local processes.

In present-day molecular clouds, about 99% of the baryonic mass exists in the gas phase, and the remaining 1% comprises of dust grains. Once these clouds become dense enough for dust grains in the clouds to shield the interstellar ultraviolet (UV) radiation, a complex chemistry can proceed (e.g., Herbst and van Dishoeck 2009). When the density becomes high enough and the temperature is low enough, gas-phase species begin to freeze out onto dust grain surfaces to form ice mantles. Consequently, in such regions, isotopic fractionation that occurred in the gas phase is imprinted in the ices (e.g., Brown and Millar 1989; Yurimoto and Kuramoto 2004). Solid-state (grain surface) reactions between molecules in the ice can further enhance or reduce the degree of isotopic fractionation. Meanwhile, desorption of molecules from the ice mantles can modify the isotope fractionation of the gas phase.

Therefore, in order to understand the isotopic fractionation in ice, and thus determine the initial conditions of small, icy bodies and planetesimals in the solar system, we need to treat the chemical interactions between gas and ice mantles on dust grains. Recently, the development of sophisticated numerical modelling considering detailed gas-phase chemical reaction networks, with grain

surface reactions, has improved our understanding of isotope chemistry in interstellar gas and ice. Together with advances in sensitivity of molecular isotopologue observations in star and planet forming regions in the era of ALMA, our ability to reconstruct the isotopic history of matter in the Galaxy has improved dramatically. Spacecraft missions to various solar system bodies, such as Stardust and Rosetta for comets 81P/Wild and 67P/Churyumov-Gerasimenko (hereafter 67P), Cassini in the Saturnian system, and Hayabusa (1 and 2) towards asteroids Itokawa and Ryugu, have brought us further information on the isotopic compositions of primitive solar system materials. Such theoretical and observational progress has made it possible to elucidate the chemical link through the history of isotopes, giving us new insights into the origins of the materials found in our solar system today.

## 1.2. Isotope ratios in star and planet forming regions and the solar system

Figure 1 summarizes the measurements of isotopic ratios D/H,  $^{12}\text{C}/^{13}\text{C}$ ,  $^{14}\text{N}/^{15}\text{N}$ , and  $^{16}\text{O}/^{18}\text{O}$  in different molecules, for various objects from prestellar/protostellar cores to protoplanetary disks around low mass stars, comets, meteorites, and planets/satellites.  $^{16}\text{O}/^{17}\text{O}$  is not plotted due to the lack of measurements compared with other isotope ratios. As mentioned, ice is formed on grain surfaces in cold and dense regions of prestellar cores. As soon as a star is formed and begins to heat the surrounding material, the dust temperature exceeds the sublimation temperature of molecules in the ice close to the protostar, and the molecules are released into the gas (e.g., *Herbst and van Dishoeck* 2009). In order to compare with solar system objects, for some observations of protostellar objects (labelled ‘warm gas’ in the figure), molecular species which are expected to be sublimated from ice are selected. Radial distributions of isotope ratios have been observed towards some protoplanetary disks (see Section 3 for details), but the averaged values are plotted in the figure.

The deuterium-to-hydrogen (D/H) ratio in water is of particular interest in the context of the origin of water on Earth and other terrestrial-type bodies. Despite significant diversity, the D/H ratios of water in comets and the bulk of meteorites are quite similar to that of terrestrial ocean water (see Section 4 and 6 for more details), in particular, with respect to the Vienna Standard Mean Ocean Water (VSMOW) value of  $1.56 \times 10^{-4}$ . The water D/H ratio in protostellar cores in clustered star-forming regions is similar to the high end of the water D/H ratio in comets (e.g., *Persson et al.* 2014), while the water D/H ratio in isolated protostellar cores is higher than that in comets (*Jensen et al.* 2019, 2021). This may be consistent with the scenario that the Sun was born in clustered star-forming regions (*Adams* 2010), assuming that little or no processing of water occurs between the protostellar stage and the formation of planetesimals and comets (*Persson et al.* 2014; *Jensen et al.* 2019). Meanwhile, deuterium ratios of organics are known to have

higher values in protostellar objects, protoplanetary disks and comets (see Section 2). We note that water is usually the dominant component of ice in molecular clouds, disks, and comets, and fractional abundances of organic species relative to water are often smaller by more than two orders of magnitude. The D/H ratios of  $\text{H}_2$  gas in the atmospheres of giant planets are close to the reference (Solar) value, as expected given their accretion from a similar reservoir of nebular gas. Larger D/H ratios of the more evolved atmospheres of the inner planets occur as a result of differing atmospheric escape rates for isotopes of different masses (see Section 5).

Nitrogen species related to  $\text{N}_2$  (e.g.,  $\text{N}_2\text{H}^+$ ) are  $^{15}\text{N}$ -poor while HCN is  $^{15}\text{N}$ -rich in protostellar objects and protoplanetary disks, which is qualitatively consistent with the theoretical prediction caused by isotope-selective photodissociation (see Section 2 and 3). Solar system objects have a  $^{15}\text{N}$ -rich value partly due to the inheritance of interstellar material, and partly due to local processes in the solar system (see Sections 5 and 6 for details). The exception is the atmospheres of gas giants whose nitrogen isotope ratios are close to the Solar reference value, probably keeping the value of the nebular gas.

Carbon and oxygen isotope ratios have relatively small variations among the solar system objects while they have large variations among the prestellar cores, depending on the species (see below). However, it is known that oxygen isotopes in meteorites in the solar system have systematic (but mass-independent) variations, which are interpreted by isotope selective photodissociation in molecular clouds/protosolar nebula (see Section 6 for details).

We note that there are deviations in the reference isotope ratios between the local interstellar medium and the solar system. Elements heavier than hydrogen and helium, such as carbon, nitrogen, and oxygen, are produced in the interiors of stars through nuclear syntheses of hydrogen, which also determine their elemental isotope ratios (e.g., *Romano et al.* 2019). Therefore, the reference (elemental) isotope ratios evolve with the chemical evolution of the galaxies, and depend on the local star formation activity in the galaxies. The solar system was formed 4.5 billion years ago when heavier isotopes were less abundant than in the present-day local interstellar medium. Also, it is observationally known that the elemental isotope ratios have gradients inside our Galaxy depending on the distance from the Galactic Center, which can be reproduced by Galactic chemical evolution models and reflects the star formation activities in our Galaxy (e.g., *Adande and Ziurys* 2012; *Zhang et al.* 2015; *Colzi et al.* 2018; *Yan et al.* 2019). Meanwhile, the observed reference (elemental) isotope ratios are not always consistent among different environments, for example, between diffuse and dense clouds. Measurements of isotope ratios are based on observations of molecular isotopologue lines, and we need to be careful about scatter of observed values caused by various processes/assumptions, such as fractionation due to chemical reactions (isotope selective photodissociation and exchange reactions), hyperfine anoma-

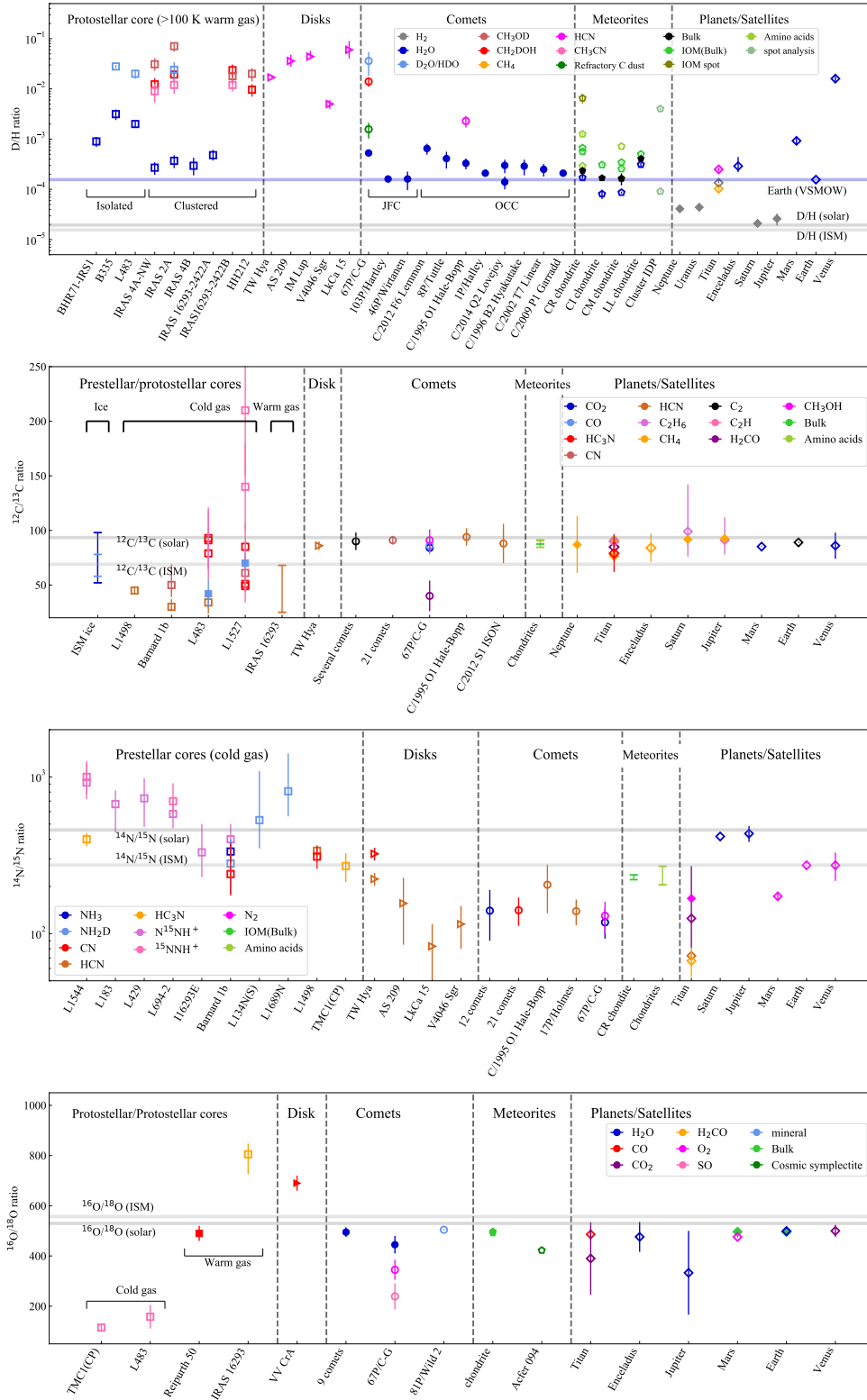


Fig. 1.— Measurements of isotope ratios of D/H, <sup>12</sup>C/<sup>13</sup>C, <sup>14</sup>N/<sup>15</sup>N, and <sup>16</sup>O/<sup>18</sup>O for various objects, including prestellar/protostellar objects, protoplanetary disks, comets, meteorites, and planets/satellites. Different colors represent different molecules and different symbols show different types of object. Data points with error bars (1σ) or ranges among multiple objects or various molecules are plotted. Filled symbols show the dominant reservoir for a given element/object. Gray horizontal lines show reference (elemental) isotope ratios in the local ISM and in the solar system. Literature sources for these data are listed at [https://sci.nao.ac.jp/MEMBER/hnomura/ppvii\\_isotope/table.pdf](https://sci.nao.ac.jp/MEMBER/hnomura/ppvii_isotope/table.pdf)

lies (e.g., *Daniel et al.* 2013; *Magalhães et al.* 2018), and excitation of transition lines (e.g., *Hily-Blant et al.* 2017). Indirect measurements of isotope ratios, for example, deriving HCN/HC<sup>15</sup>N ratios from H<sup>13</sup>CN/HC<sup>15</sup>N observations with assuming the <sup>12</sup>C/<sup>13</sup>C ratios, also can introduce significant scatter (*Roueff et al.* 2015; *Hily-Blant et al.* 2020).

## 2. ISOTOPE FRACTIONATION CHEMISTRY

This section reviews the basic processes of isotope fractionation of volatile elements (H, C, N, and O) in star- and planet forming regions. As a guide, Figure 2 shows the chemical evolution in a forming and evolving molecular cloud predicted by a gas-grain astrochemical model with H, C, N, O isotope fractionation chemistry. The physical model of the cloud is based on the 1-D shock model of *Bergin et al.* (2004), which mimics the scenario that molecular clouds are formed due to the compression of diffuse HI gas by super-sonic accretion flows (*Inutsuka et al.* 2015). As time proceeds, the column density of post-shock materials (i.e., molecular cloud) increases, which assists molecular formation by attenuating the interstellar UV radiation. As such, the horizontal axes in Fig. 2 can be read as time ( $A_v = 1$  mag corresponds to  $\sim 3$  Myr in this particular model). The gas density and temperature of the cloud is  $\sim 10^4$  cm<sup>-3</sup> and 10-20 K, respectively (Fig 2a). The chemical model is based on the gas-grain model presented by *Furuya and Aikawa* (2018), where H and N isotope fractionation were studied, and is extended to include O and C isotope fractionation chemistry. In general, there are two mechanisms to cause isotope fractionation in gas-phase molecules: isotope exchange reactions and isotope selective photodissociation. Both mechanisms are included in the model, with up to date rate coefficients (e.g., *Roueff et al.* 2015; *Loison et al.* 2019b; *Colzi et al.* 2020; *Loison et al.* 2020). As explained below, the dominant fractionation pathways of H and C isotopes are triggered by isotope exchange reactions (Sections 2.1 and 2.3), while those for O and N isotopes are triggered by isotope selective photodissociation (Section 2.2 and 2.4).

### 2.1. Deuterium fractionation

In star- and planet-forming regions, hydrogen and deuterium are primarily present as H<sub>2</sub> and HD, respectively. Deuterium fractionation can be understood as the process that redistributes deuterium from HD into other species (see also *Ceccarelli et al.* 2014, for the review of deuterium fractionation chemistry). In molecular clouds/cores, deuterium fractionation is mainly triggered by the isotope exchange reaction,  $\text{H}_3^+ + \text{HD} \rightleftharpoons \text{H}_2\text{D}^+ + \text{H}_2$  (e.g., *Watson* 1976; *Dalgarno and Lepp* 1984). The backward reaction is endothermic by 0-256 K (the actual value differs depending on the nuclear spin state of H<sub>2</sub>: ortho-H<sub>2</sub> or para-H<sub>2</sub>, see below), so thermal energy is required for it to proceed (*Hugo et al.* 2009). Thus the rate coefficient of the backward reaction is much lower than that of the forward reaction at low gas temperatures ( $\lesssim 30$  K). This leads to H<sub>2</sub>D<sup>+</sup> becom-

ing more abundant over time with respect to H<sub>3</sub><sup>+</sup>. Since the H<sub>3</sub><sup>+</sup> isotopologues play a central role in the production of a variety of interstellar molecules (*Herbst and Klemperer* 1973), the deuterium enrichment in H<sub>3</sub><sup>+</sup> is transferred to all the other molecules in the gas phase and on grain surfaces (Fig. 2). For example, N<sub>2</sub>D<sup>+</sup>/N<sub>2</sub>H<sup>+</sup> ratio reaches to  $>0.1$  in prestellar cores (see *Ceccarelli et al.* 2014, for the review of the observations of deuterated species towards prestellar cores). Chemical species that destroy H<sub>2</sub>D<sup>+</sup> (e.g., CO and N<sub>2</sub>) are readily frozen out onto cold dust grain surfaces, further enhancing the deuterium enrichment at low temperatures. This is consistent with the higher D/H ratio in methanol (CH<sub>3</sub>OH) than water observed in the warm gas ( $>100$  K) around protostars, where ices have sublimated; methanol is formed via a sequential hydrogenation of CO on grain surfaces, while water is predominantly formed via a sequential hydrogenation of O on grain surfaces prior to the CO freeze-out (*Cazaux et al.* 2011; *Taquet et al.* 2014; *Furuya et al.* 2016).

At warm temperatures ( $\gtrsim 30$  K), other exchange reactions, such as  $\text{CH}_3^+ + \text{HD} \rightleftharpoons \text{CH}_2\text{D}^+ + \text{H}_2$ , which have higher endothermicity ( $\lesssim 500$  K, again the value depends on the nuclear spin state of H<sub>2</sub>) than the H<sub>2</sub>D<sup>+</sup> pathway, become the main driver of deuterium fractionation (*Millar et al.* 1989; *Roueff et al.* 2013; *Nyman and Yu* 2019). Spatially resolved observations of deuterated molecules in protoplanetary disks with ALMA have indicated that both the H<sub>2</sub>D<sup>+</sup> pathway and the higher-temperature pathways are operating in disks (e.g., *Huang et al.* 2017; *Salinas et al.* 2017; *Cataldi et al.* 2021, see Section 3.1).

In addition to the gas temperature, the spin temperature of H<sub>2</sub> (i.e., the ortho-to-para abundance ratio; OPR) is another key quantity that controls deuterium fractionation (*Pagani et al.* 1992; *Flower et al.* 2006; *Taquet et al.* 2014; *Sipilä et al.* 2017). The internal energy of ortho-H<sub>2</sub> is higher than that of para-H<sub>2</sub> by 170.5 K, which helps to overcome the endothermicity of the backward exchange reactions. Even when the H<sub>2</sub> OPR is small,  $\sim 10^{-3}$ , H<sub>2</sub> rather than CO is the main destroyer of H<sub>2</sub>D<sup>+</sup> and thus deuterium fractionation can be slowed down (*Furuya et al.* 2015). When H<sub>2</sub> is formed by grain surface reactions, the H<sub>2</sub> OPR corresponds to the statistical value of three (*Watanabe et al.* 2010), but its value can fall over time via nuclear spin conversion in the gas phase, through proton transfer reactions (e.g.,  $\text{o-H}_2 + \text{H}^+ \rightleftharpoons \text{p-H}_2 + \text{H}^+$ ) (*Hugo et al.* 2009; *Honvault et al.* 2011), and on grain surfaces (*Ueta et al.* 2016; *Tsuge et al.* 2019, 2021). Astrochemical models with nuclear spin conversion of H<sub>2</sub> at the formation stage of molecular clouds predict that the H<sub>2</sub> OPR is already much lower than the statistical value of three, when the main component of the gas becomes H<sub>2</sub> molecules (*Furuya et al.* 2015; *Lupi et al.* 2021). H<sub>2</sub> molecules are not easily observable, and the H<sub>2</sub> OPR has been estimated from observations of molecules other than H<sub>2</sub>, such as N<sub>2</sub>D<sup>+</sup> and H<sub>2</sub>D<sup>+</sup>, as their abundances depend on the the H<sub>2</sub> OPR. Observational studies have so far consistently suggested that the H<sub>2</sub> OPR is much lower than unity ( $10^{-4}$ –0.1) in the cold gas of prestellar cores and

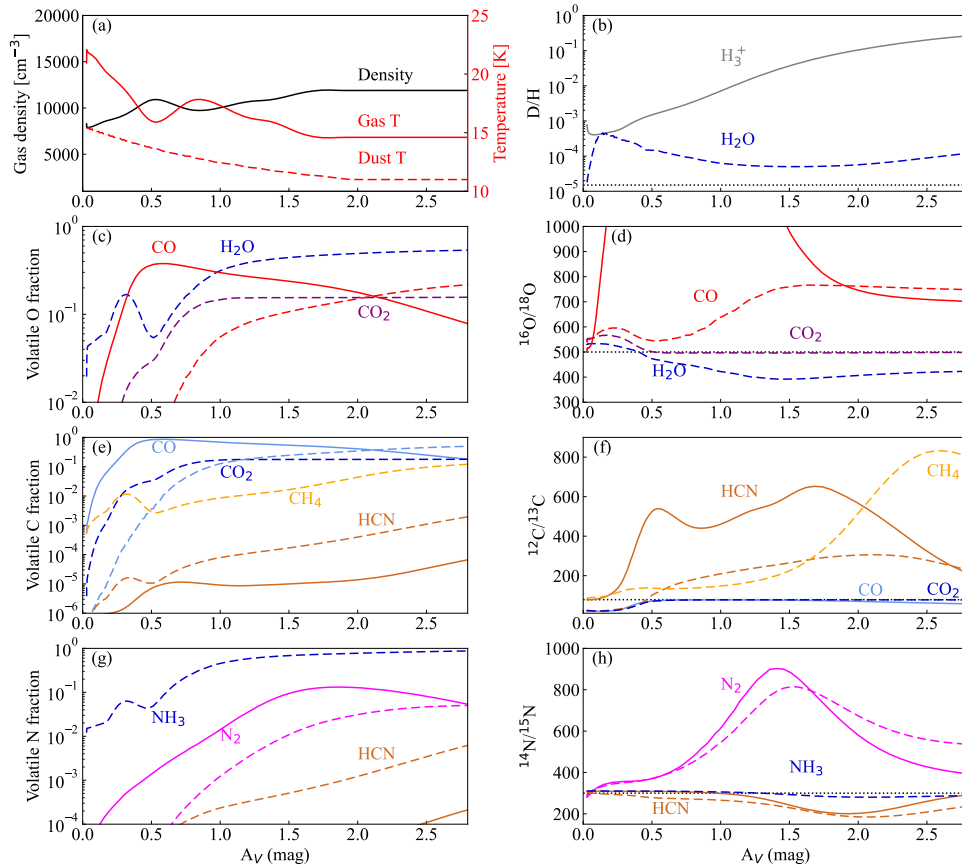


Fig. 2.— Chemical evolution in a molecular cloud predicted by a gas-grain astrochemical model with H, C, N, O isotope fractionation chemistry (Furuya and Aikawa 2018, with some updates). Panel (a) shows physical evolution as a function of visual extinction ( $A_V$ ). Panels (c), (e), and (g) show the fraction of volatile elements locked up in selected chemical species, while panels (b), (d), (f), and (h) show the degree of isotope fractionation. Solid lines represent gas-phase species, while dashed lines represent icy species. Black dotted lines in the right panels show the reference (elemental) isotope ratios adopted in the model.

protostellar envelopes (e.g., Pagani et al. 2011; Brünken et al. 2014; Harju et al. 2017).

Deuterium fractionation occurs primarily as a result of gas phase processes, but grain surface reactions at low temperatures ( $\sim 10$  K) can further enhance the level of fractionation (Watanabe and Kouchi 2008; Fedoseev et al. 2015). The degree of deuterium fractionation of formaldehyde and methanol can be enhanced by the substitution and abstraction reactions of H and D atoms at  $\sim 10$  K after their formation (Watanabe and Kouchi 2008; Taquet et al. 2012; Cooper and Kästner 2019). As other examples, methylamine ( $\text{CH}_3\text{NH}_2$ ) and ethanol ( $\text{CH}_3\text{CH}_2\text{OH}$ ) are also subject to the H/D substitution reactions (Oba et al. 2014, 2016). Moreover, the efficiency of the substitution and abstraction reactions depends on the molecular functional group, e.g., deuterium substitution can be effective in the  $\text{CH}_3$ -group of methanol but less so in its OH-group. This can result in a high  $\text{CH}_2\text{DOH}/\text{CH}_3\text{OD}$  ratio ( $>1$ ), as observed in the warm gas of embedded low-mass protostars (Taquet et al. 2012). In contrast, once water is formed, it does not efficiently react with D atoms to be deuterated

(Nagaoka et al. 2005). In addition, several laboratory studies showed that H–D exchanges between hydrogen-bonded molecules in mixed ices occur efficiently at warm temperatures ( $\gtrsim 70$  K) (Ratajczak et al. 2009; Faure et al. 2015; Lamberts et al. 2015). See the discussion in Furuya et al. (2016) for further details.

In the innermost regions of protoplanetary disks, where gas temperatures are greater than  $\sim 500$  K, isotope exchange reactions between deuterated species with  $\text{H}_2$ , such as  $\text{HDO} + \text{H}_2 \rightleftharpoons \text{H}_2\text{O} + \text{HD}$  and  $\text{CH}_3\text{D} + \text{H}_2 \rightleftharpoons \text{CH}_4 + \text{HD}$  (with activation energy barriers of 5170 K and 4600 K, respectively), could reduce the degree of dueteration (Richet et al. 1977; Lécluse and Robert 1994). Presently, however, there are no observational constraints on the D/H ratio of water in protoplanetary disks.

## 2.2. Oxygen isotope fractionation

In contrast to deuterium fractionation, which is powered by isotope exchange reactions, oxygen isotope fractionation is thought to be caused by isotope selective photodis-

sociation of CO, followed by the formation of water ice (e.g., Clayton 2002; Yurimoto and Kuramoto 2004; Lyons and Young 2005). CO photodissociation is subject to self-shielding (i.e., CO itself can be the dominant absorber of dissociating UV radiation instead of dust grains). Because rarer isotopologues (e.g., C<sup>18</sup>O and C<sup>17</sup>O) are less abundant, they are not self-shielded until deeper into the cloud or the disk. This makes CO photodissociation an isotope-selective process (e.g., Visser et al. 2009; Miotello et al. 2014). See also Chakraborty et al. (2018) for the experiments of photodissociation of the CO isotopologues. The underabundance of C<sup>18</sup>O with respect to <sup>12</sup>CO or <sup>13</sup>CO due to the isotope selective photodissociation has been observed in molecular clouds illuminated by UV photons from nearby stars (e.g., Shimajiri et al. 2014; Li et al. 2018; Yamagishi et al. 2019) and in a protoplanetary disk (Smith et al. 2009). As a result of isotope selective photodissociation of CO, <sup>17,18</sup>O-enriched atomic oxygen is produced and can be converted into water ice. Then the two major reservoirs of volatile oxygen, CO and water can have different isotope compositions; the former is depleted in heavy oxygen isotopes, while the latter shows the opposite trend (see Fig. 2d). There is no constraint on oxygen isotope fractionation of water in star- and planet-forming regions. Cometary water, which could originate from the parent molecular cloud of the solar system (e.g., Cleaves et al. 2014; Altwegg et al. 2017), is enriched in <sup>18</sup>O (see Section 4.4).

Oxygen isotope compositions of other minor O-bearing species (i.e., neither CO nor H<sub>2</sub>O) would depend on the source of oxygen from which they form. For example, it is expected that CH<sub>3</sub>OH and H<sub>2</sub>CO are depleted in heavy oxygen isotopes, as they are formed via sequential reactions of atomic hydrogen with CO on grain surfaces (e.g., Watanabe and Kouchi 2002; Fuchs et al. 2009). Note that in contrast to deuterium fractionation, there is no clear evidence that grain surface reactions modify the degree of oxygen isotope fractionation (Cooper and Kästner 2019). CO<sub>2</sub>, which is mainly formed via CO + OH → CO<sub>2</sub> + H on grain surfaces, is expected to show no oxygen isotope fractionation, as OH is formed by the photodissociation of water ice and/or the hydrogenation of atomic oxygen (dashed orange line in Fig. 2).

Loison et al. (2019b) explored the impact of isotope exchange reactions on oxygen isotope fractionation under the physical conditions appropriate for dense molecular clouds. They found that the gas-phase O-bearing species could be fractionated by isotope exchange reactions, such as <sup>18</sup>O + XO ⇌ O + X<sup>18</sup>O + ΔE, where X is either O, N, or S and ΔE ≈ 30–40 K, when atomic oxygen is moderately abundant (≥10<sup>-5</sup> with respect to H<sub>2</sub>). The astrochemical model of Loison et al. (2019b) successfully reproduced the <sup>18</sup>O enrichment in SO observed in cold dense cores. It should be noted, however, that high abundance of atomic oxygen in the gas phase leads to the formation of O<sub>2</sub> (e.g., Hincelin et al. 2011), while the detection of O<sub>2</sub> in cold clouds is rare (Goldsmith et al. 2000; Pagani et al. 2003; Liseau et al. 2012). A unique feature of oxygen is that it has three sta-

ble isotopes whereas hydrogen, carbon and nitrogen have only two stable isotopes. As a result, in principle, effects by isotope selective reactions could be resolved from those by isotope exchange reactions by comparing the <sup>18</sup>O/<sup>16</sup>O ratio with the <sup>17</sup>O/<sup>16</sup>O ratio (see Section 5).

In very inner regions of protoplanetary disks, where gas temperature is greater than ~500 K, oxygen isotope exchange can occur between silicates and H<sub>2</sub>O gas (see Section 6).

### 2.3. Carbon isotope fractionation

Carbon isotope fractionation occurs via isotope selective photodissociation of CO (e.g., Visser et al. 2009) and an exothermic isotope exchange reaction: CO + <sup>13</sup>C<sup>+</sup> ⇌ <sup>13</sup>CO + C<sup>+</sup> + 35 K (e.g., Watson 1976; Langer et al. 1984). PDR models have predicted that the former is less important than the latter, because the former is efficient only at ~1 A<sub>V</sub> (Röllig and Ossenkopf 2013). Astrochemical models under dark cloud physical conditions have predicted that carbon-bearing molecules are divided into two groups from the view point of <sup>13</sup>C fractionation via the isotope exchange reaction (e.g., Langer et al. 1984): CO and molecules formed from CO (e.g., CO<sub>2</sub> and CH<sub>3</sub>OH) are enriched in <sup>13</sup>C, while molecules formed from C<sup>+</sup> (e.g., HCN, CN and CH<sub>4</sub>) are <sup>13</sup>C-poor (Fig. 2f). However, because CO is the main reservoir of volatile carbon, the <sup>13</sup>C enrichment of CO cannot be large. On the other hand, HCO<sup>+</sup> is affected by another exchange reaction, <sup>13</sup>CO + HCO<sup>+</sup> ⇌ CO + H<sup>13</sup>CO<sup>+</sup> + 17.8 K (Langer et al. 1984; Mladenović and Roueff 2017), and consequently, HCO<sup>+</sup> becomes further enriched in <sup>13</sup>C compared to CO.

The above mentioned scenario is challenged by the measurements of <sup>12</sup>C/<sup>13</sup>C ratios of CN and HCN in dense clouds, which suggest these nitriles are enriched in <sup>13</sup>C (Daniel et al. 2013; Magalhães et al. 2018, Fig. 1). Recent quantum chemical calculations have identified several other isotope exchange reactions, such as <sup>13</sup>C + HCN ⇌ C + H<sup>13</sup>CN + 48 K and <sup>13</sup>C + C<sub>3</sub> ⇌ C + <sup>13</sup>CC<sub>2</sub> + 28 K (Roueff et al. 2015; Colzi et al. 2020; Loison et al. 2020). The newly identified exchange reactions modify the classical picture mentioned above; nitriles and carbon-chain molecules can be enriched in <sup>13</sup>C depending on physical environments as demonstrated by the gas-grain astrochemical model of dense cores with A<sub>V</sub> = 10 mag in (Loison et al. 2020). Although these new isotope exchange reactions are taken into account in the model shown in Fig. 2, HCN is depleted in <sup>13</sup>C, likely because the model only considers the regions where A<sub>V</sub> is not high (<3 mag) and the interstellar radiation field is not fully shielded.

Oxygen-bearing complex organic molecules (COMs, e.g., glycolaldehyde and dimethyl ether) in the warm gas around protostars IRAS 16293-2422, where ices have sublimated are enriched in <sup>13</sup>C by up to a factor of 2 compared to the elemental ratio in the local ISM (Jørgensen et al. 2016, 2018, Fig. 1). COMs are thought to form on warm (≥20 K) dust grains irradiated by UV (e.g., Herbst and van

*Dishoeck* 2009). The enrichment of  $^{13}\text{C}$  in COMs might be due to slightly higher binding energy of  $^{13}\text{CO}$  than  $^{12}\text{CO}$  (i.e., resident time of  $^{13}\text{CO}$  on grains is longer than  $^{12}\text{CO}$ ) and/or the effect of stellar UV radiation, which produces  $^{13}\text{C}$  enriched atomic C by isotope selective photodissociation of CO (*Jørgensen et al.* 2018).

In addition to the measurements of  $^{12}\text{C}/^{13}\text{C}$  ratio in various molecules, observations in molecular clouds have found that the abundances of the  $^{13}\text{C}$  isotopomers (i.e., species with the same chemical formula, but differing in the position of  $^{13}\text{C}$ ) depend on which carbon atom in a molecule is substituted by  $^{13}\text{C}$  (e.g., *Takano et al.* 1998; *Sakai et al.* 2007, 2010; *Taniguchi et al.* 2019; *Giesen et al.* 2020). For example, the abundance ratio of  $^{13}\text{CCH}$  to  $\text{C}^{13}\text{CH}$  is greater than unity (i.e., more stable isotopomer  $^{13}\text{CCH}$  is more abundant than  $\text{C}^{13}\text{CH}$ ) in dense molecular clouds (*Sakai et al.* 2010; *Taniguchi et al.* 2019). These isotopomer ratios provide a clue of the formation pathway of the molecules or indicate the efficient position exchange reaction, which converts less stable isotopomers to more stable ones at low temperatures (e.g., see *Sakai et al.* 2010; *Furuya et al.* 2011, for the case of CCH).

#### 2.4. Nitrogen isotope fractionation

According to observations towards dense clouds, there is no clear evidence of nitrogen isotope fractionation in the gas phase nitriles (*Hily-Blant et al.* 2020, and references therein), while ammonia and  $\text{N}_2\text{H}^+$  in the gas phase show significant  $^{15}\text{N}$  depletion by a factor of  $\sim 2\text{--}3$  compared to the elemental ratio in the local ISM (*Bizzocchi et al.* 2013; *Redaelli et al.* 2018, Fig. 1). The significant depletion of  $^{15}\text{N}$  in  $\text{N}_2\text{H}^+$  indicates that its parent molecule,  $\text{N}_2$ , is also depleted in  $^{15}\text{N}$ . To the best of our knowledge, there are no direct measurements of the  $^{14}\text{N}/^{15}\text{N}$  ratio in any molecules in the hot ( $>100$  K) gas, where ices have sublimated. Therefore, the  $^{14}\text{N}/^{15}\text{N}$  ratio of molecular ices in the ISM is presently not constrained. On the other hand, observations of comets in our solar system have found that HCN and  $\text{NH}_3$  in cometary ices are enriched in  $^{15}\text{N}$  compared to the solar wind, by a factor of  $\sim 2\text{--}3$  (see Section 4.3).

Compared to the other volatile elements, the mechanism of nitrogen isotope fractionation remains an open question. Previously, it had been suggested that nitrogen isotope exchange reactions are efficient at low temperatures ( $\sim 10$  K), so gas-phase nitriles and ammonia can be enriched in  $^{15}\text{N}$ , and the gas-phase enrichment transferred to the ice ( $\sim 10$  K; e.g. *Terzieva and Herbst* 2000; *Charnley and Rodgers* 2002; *Wirström et al.* 2012). However, recent reinvestigations of the exchange reactions by quantum chemistry calculations and astrochemical simulations have found that fractionation by exchange reactions is much less efficient than had previously thought even at 10 K (*Roueff et al.* 2015; *Wirström and Charnley* 2018; *Loison et al.* 2019a). The updated models are consistent with observations in dense clouds that the degree of nitrogen isotope fractionation is generally small. However, a major puzzle remains regarding the

depletion of  $^{15}\text{N}$  in  $\text{N}_2\text{H}^+$ ; this is difficult to explain using isotope-exchange reactions, which should produce the opposite trend. To explain the  $^{15}\text{N}$  depletion of  $\text{N}_2\text{H}^+$ , *Loison et al.* (2019a); *Hily-Blant et al.* (2020) have proposed the possibility that the rates of dissociative recombination ( $\text{N}_2\text{H}^+ + e^- \rightarrow \text{N}_2 + \text{H}$ ) for  $\text{N}^{15}\text{NH}^+$  and  $^{15}\text{NNH}^+$  are larger than that for  $^{14}\text{N}_2\text{H}^+$  (see the original papers for details). This reaction is one of the main destruction pathways of  $\text{N}_2\text{H}^+$ . As noted by those authors, there are no experimental measurements of the dissociative recombination rates for  $\text{N}^{15}\text{NH}^+$  and  $^{15}\text{NNH}^+$  at low temperatures ( $\sim 10$  K). Experimental or/and theoretical studies will therefore be required to verify the scenario. In the model in Fig. 2, the two relevant rate coefficients are assumed to be the same.

Alternatively, nitrogen isotope fractionation could be induced by isotope selective photodissociation of  $\text{N}_2$ , followed by the formation of  $^{15}\text{N}$  enriched N-bearing icy species, such as  $\text{NH}_3$  and HCN ices (*Furuya and Aikawa* 2018, Fig. 2h). See *Heays et al.* (2014) and *Chakraborty et al.* (2014, 2016) for theory and experiments of the isotope selective photodissociation of  $\text{N}_2$ , respectively. This mechanism is an analog of oxygen isotope fractionation induced by isotope selective photodissociation of CO, followed by  $\text{H}_2\text{O}$  ice formation (compare Fig. 2d and 2h). A model by *Furuya and Aikawa* (2018), which simulates the nitrogen isotope fractionation during the formation and evolution of a molecular cloud via the compression of diffuse atomic gas, could qualitatively explain the  $^{15}\text{N}$  depletion in  $\text{N}_2\text{H}^+$  and the  $^{15}\text{N}$  enrichment in cometary ices (assuming cometary volatile was inherited from the ISM), but could not reproduce them quantitatively; the model predicted that the degree of fractionation is up to several tens of per-cent. However, their model is based on a specific physical situation. More numerical studies, and varying physical parameters, are necessary to better understand the  $^{15}\text{N}$  observations. We note that if the isotope selective photodissociation is the main cause of nitrogen isotope fractionation,  $\text{N}_2$  would need to be the main gas-phase reservoir of elemental nitrogen; otherwise isotope selective photodissociation of  $\text{N}_2$  does not work (*Furuya and Aikawa* 2018). Then, the uncertainty in the mechanism of the nitrogen isotope fractionation is linked to our uncertainty regarding the main nitrogen reservoirs in the ISM.

### 3. PROTOPLANETARY DISKS

Chemistry in protoplanetary disks can be described by analogy with that of molecular clouds. Isotope fractionation due to isotope exchange reactions proceeds in the cold outer regions of disks, while isotope selective photodissociation takes place in the surface layer of the disks, which is directly irradiated by stellar UV radiation. The dust grains in disks are the building blocks of planets/asteroids/comets in planetary systems. They collisionally grow and move in vertical and radial directions inside the disks; settling towards the disk midplane and radially migrating towards/away from the central stars, depending the direction of gas pressure

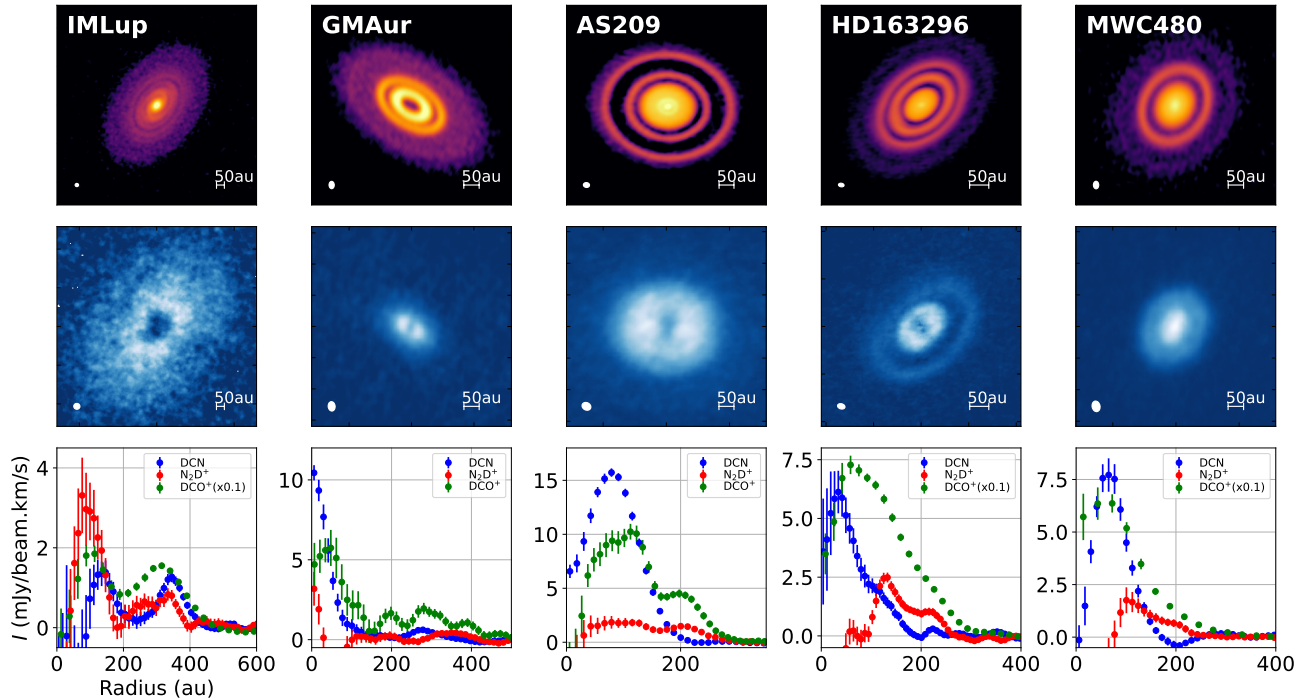


Fig. 3.— Dust continuum images (top), integrated line images of HCN 3-2 (middle), radial profiles of deuterated species (bottom) towards five bright protoplanetary disks (Öberg et al. 2021a; Cataldi et al. 2021). DCN, DCO<sup>+</sup>, and N<sub>2</sub>D<sup>+</sup> are located from inner to outer regions in this order for most disks.

gradient force. This differs from the situation in molecular clouds where dust grains are small and coupled with the gas motion. Isotope ratios could trace how and where the objects in planetary systems are formed in disks.

### 3.1. Cold and warm paths of deuteration in disks

HCO<sup>+</sup> and HCN have the strongest emission lines of hydrogen containing species towards protoplanetary disks. The deuterated species, DCO<sup>+</sup>, was initially detected using single dish telescopes (van Dishoeck et al. 2003; Guilloteau et al. 2006), and a tentative detection of DCN by JCMT was confirmed by Submillimeter Array (SMA) observations (Thi et al. 2004; Qi et al. 2008). The subsequent SMA and IRAM PdBI survey observations detected DCO<sup>+</sup> towards more objects (e.g., Öberg et al. 2010, 2011; Teague et al. 2015) and now ALMA has revealed detailed spatial distributions of both DCO<sup>+</sup> and DCN in disks.

Since deuterium fractionation is driven by isotope exchange reactions (see Section 2.1), the enhancement of the D fractionation in the cold outer disks has been theoretically suggested and observationally confirmed especially for DCO<sup>+</sup> (e.g., Aikawa and Herbst 1999, 2001; Qi et al. 2008). On the other hand, HCO<sup>+</sup> and DCO<sup>+</sup> deplete if gas-phase CO is frozen out on grains since HCO<sup>+</sup> is formed by protonation of CO. Therefore, it is expected that DCO<sup>+</sup> is enhanced most around the CO snowline inside which CO exists in the gas-phase without freezing on dust grains, and ALMA observations with high spatial resolution have ac-

tually revealed it (e.g., Mathews et al. 2013; Salinas et al. 2017). In addition, ring-like enhancements of DCO<sup>+</sup> in the outer disk are explained by photodesorption of CO (e.g., Öberg et al. 2015). Meanwhile, ALMA observations also show that both DCN and DCO<sup>+</sup> exist in the inner disk, with DCN distributed in more inner disks compared with DCO<sup>+</sup>, suggesting warm formation paths for deuterated species (e.g., Huang et al. 2017; Kastner et al. 2018; Öberg et al. 2021b; Cataldi et al. 2021, , see Figure 3). Theoretical models show that DCN and DCO<sup>+</sup> can be formed through, for example, N + CHD/DCO → DCN + H/O and CH<sub>4</sub>D<sup>+</sup> + CO → DCO<sup>+</sup> + CH<sub>4</sub>, respectively in addition to the cold path induced by H<sub>3</sub><sup>+</sup> + HD ⇌ H<sub>2</sub>D<sup>+</sup> + H<sub>2</sub> (e.g., Cleeves et al. 2016; Aikawa et al. 2018).

N<sub>2</sub>D<sup>+</sup> has also been detected in protoplanetary disks by ALMA (Huang et al. 2017; Salinas et al. 2017; Cataldi et al. 2021). N<sub>2</sub>D<sup>+</sup> is mainly distributed in the outer disks (Figure 3), consistent with the theoretical models which predict that only the cold pathway is efficient for N<sub>2</sub>D<sup>+</sup> formation. High deuterium fractionation of N<sub>2</sub>D<sup>+</sup>/N<sub>2</sub>H<sup>+</sup> ∼ 0.1 – 1, compared with DCO<sup>+</sup>/HCO<sup>+</sup> and DCN/HCN ∼ 0.01 – 0.1, also reflects that N<sub>2</sub>D<sup>+</sup> is formed only in cold outer disks. C<sub>2</sub>D is another deuterated species recently detected in protoplanetary disks by ALMA (Loomis et al. 2020). C<sub>2</sub>D possibly has a radial distribution similar to that of DCO<sup>+</sup>.

HD has been detected towards protoplanetary disks by Herschel Space Observatory (Bergin et al. 2013; McClure



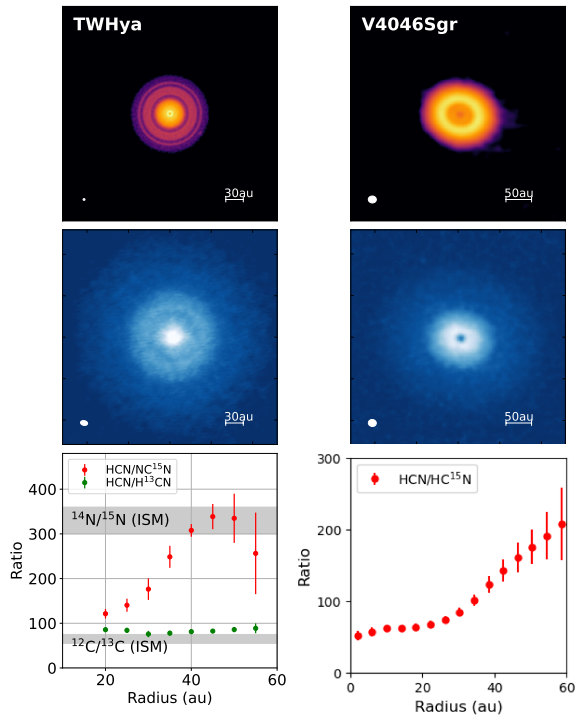


Fig. 4.— Dust continuum images (top), total integrated intensity maps of HCN(4–3) (middle) and radial profiles of  $\text{HC}^{14}\text{N}/\text{HC}^{15}\text{N}$  (TW Hya, V4046 Sgr) and  $\text{H}^{12}\text{CN}/\text{H}^{13}\text{CN}$  (TW Hya) ratios (bottom) towards nearby protoplanetary disks (cf. *Tsukagoshi et al. 2019*; *Hily-Blant et al. 2019*; *Guzmán 2021*). The  $\text{HC}^{14}\text{N}/\text{HC}^{15}\text{N}$  ratio decreases in the inner regions for both disks.

*et al. 2016*). Since  $\text{H}_2$  is the dominant reservoir of hydrogen, HD is thought not to be fractionated, maintaining its cosmic abundance of  $\sim 10^{-5}$ . As  $\text{H}_2$  line emission mainly traces relatively hot surface regions of disks, the HD lines provide a useful estimate for disk gas masses (e.g. *Trapman et al. 2017*; *Kama et al. 2020*).

Since  $\text{H}_2\text{D}^+$  is a key species which initiates the deuterium chemistry in the cold outer disks, there have been attempts to observe the species towards protoplanetary disks. However, observations failed to detect both  $\text{H}_2\text{D}^+$  and  $\text{D}_2\text{H}^+$  (e.g., *Qi et al. 2008*; *Chapillon et al. 2011*), possibly due to the concentration of D in  $\text{D}_3^+$  as is suggested by theoretical models (e.g., *Willacy and Woods 2009*). HDO is another important deuterated species which has not been detected in protoplanetary disks so far (e.g., *Guilloteau et al. 2006*), while it has been studied very well by theoretical models (e.g., *Furuya et al. 2013*; *Albertsson et al. 2014*; *Cleeves et al. 2014*). Detection of deuterated water in disks is one of the important keys to understanding the origin of water in the solar system objects linking from molecular clouds.

### 3.2. Nitrogen fractionation in disks

Nitrogen isotopes were detected in protoplanetary disks for the first time by ALMA (*Guzmán et al. 2015, 2017*;

*Hily-Blant et al. 2017, 2019*; *Booth et al. 2019*). The measured nitrogen isotope ratios,  $\text{HC}^{14}\text{N}/\text{HC}^{15}\text{N}$ , are similar to those in protostellar envelopes and comets, and  $\text{C}^{14}\text{N}/\text{C}^{15}\text{N}$  has a slightly higher value (see Figure 1). Spatially resolved  $\text{HC}^{14}\text{N}/\text{HC}^{15}\text{N}$  measurements have been obtained towards two nearby objects: TW Hya and V4046 Sgr, which show that the ratio decreases inside  $\sim 50$  au for both objects (Figure 4). Meanwhile,  $\text{HC}^{14}\text{N}/\text{HC}^{15}\text{N}$  has been measured towards disks with various ages from Class 0/I to Class II, suggesting that the ratio decreases with evolutionary stage. This could reflect an increased isotope selective photodissociation efficiency as the surrounding envelope clears (*Bergner et al. 2020*).

Nitrogen fractionation models in protoplanetary disks have been constructed (*Visser et al. 2018*; *Lee et al. 2021b*). As is shown in Section 2, nitrogen fractionation is mainly caused by isotope selective photodissociation rather than isotope exchange reactions. In the case of protoplanetary disks, the fractionation therefore proceeds mainly in the surface layer and the outer edge of the disks. Observations suggest that no clear correlation exists between the degree of deuterium and nitrogen fractionation, which is consistent with the model that deuterium and nitrogen fractionation are mainly caused by different mechanisms (exchange reactions vs. isotope selective photodissociation) (*Guzmán et al. 2017*). The fractionation depends on the properties of dust grains, that is, how much ultraviolet irradiation can penetrate deeper in the disks. The fractionation becomes significant if small dust grains are more abundant and the molecular layer shrinks (*Lee et al. 2021b*). The observed tendency for  $\text{HC}^{14}\text{N}/\text{HC}^{15}\text{N}$  to increase in the outer parts of disks could then be explained if the small dust grains deplete in the outer disk, as suggested by dust evolution models (e.g., *Birnstiel et al. 2012*).

### 3.3. Carbon and oxygen fractionation in disks

Isotopologues of CO ( $^{12}\text{C}^{16}\text{O}$ ,  $^{13}\text{C}^{16}\text{O}$ ,  $^{12}\text{C}^{18}\text{O}$ ), were the first molecules detected in protoplanetary disks, using millimeter arrays and a single dish telescope (*Kawabe et al. 1993*; *Koerner et al. 1993*; *Guilloteau and Dutrey 1994*). They emit some of the strongest lines in disks, and these lines are commonly used to survey the gaseous component of disks (e.g., *Williams and Best 2014*; *Ansdell et al. 2016*). However, since  $^{12}\text{C}^{16}\text{O}$  lines are optically thick, it is difficult to measure the isotope ratios, using these lines. Together with observations of  $^{13}\text{C}^{16}\text{O}$ ,  $^{12}\text{C}^{18}\text{O}$ ,  $^{12}\text{C}^{17}\text{O}$  lines and multi-transition lines of  $^{12}\text{C}^{16}\text{O}$ , CO isotope ratios are measured toward the disk around HD 163296 by fitting observations to model calculations (*Qi et al. 2011*). The derived values are consistent with the ISM values. Another measurement has been taken toward a protoplanetary disk around VV CrA, using high-dispersion infrared spectroscopic observations of CO ro-vibrational line absorption (*Smith et al. 2009*). The measured values are  $^{12}\text{C}^{16}\text{O}/^{12}\text{C}^{18}\text{O} = 690 \pm 30$ ,  $^{12}\text{C}^{16}\text{O}/^{12}\text{C}^{17}\text{O} = 2800 \pm 300$ , and  $^{12}\text{C}^{18}\text{O}/^{12}\text{C}^{17}\text{O} = 4.1 \pm 0.4$ , which are not signifi-

cantly different from the ISM values. ALMA and IRAM NOEMA have also made it possible to detect the rarer isotopologues  $^{13}\text{C}^{18}\text{O}$  and  $^{13}\text{C}^{17}\text{O}$  from protoplanetary disks (Zhang et al. 2017, 2020; Booth et al. 2019; Booth and Ilee 2020).  $^{12}\text{C}/^{13}\text{C} = 40_{-6}^{+9}$  is suggested toward the TW Hya disk by fitting model calculations to the observations. These observations of optically thin CO isotopologues are often used as mass tracers by simply assuming that there is no significant fractionation in carbon and oxygen isotopes.

$\text{H}^{13}\text{CO}^+$  has been detected by single-dish and SMA observations toward a protoplanetary disks (Thi et al. 2004; Qi et al. 2008). ALMA has made it possible to spatially resolve both  $\text{H}^{13}\text{CO}^+$  and  $\text{H}^{13}\text{CN}$  towards some disks (Guzmán et al. 2015, 2017; Huang et al. 2017; Booth et al. 2019; Hily-Blant et al. 2019). Since the corresponding  $\text{HCO}^+$  and  $\text{HCN}$  lines are optically thick however, it is fundamentally difficult to measure the isotope ratios directly. However, the disks become optically thinner at large radii, and a low  $\text{H}^{12}\text{CO}^+/\text{H}^{13}\text{CO}^+$  ratio is measured in the outer edge of the HD 97048 disk by fitting observations with model calculations (Booth et al. 2019). Also, taking advantage of optically thin hyper-fine lines of  $\text{HCN}$ ,  $^{12}\text{C}/^{13}\text{C}$  in  $\text{HCN}$  is measured towards the TW Hya disk, showing  $^{12}\text{C}/^{13}\text{C} = 86 \pm 4$  on average, which is slightly higher than the ISM value, and the radial dependence is not high (from  $\sim 75.9 \pm 7.0$  to  $\sim 88.7 \pm 11.1$ ) throughout the disk inside 55 au — significantly different from the  $\text{HC}^{14}\text{N}/\text{HC}^{15}\text{N}$  ratio (Hily-Blant et al. 2019, Figure 4). Carbon isotope models of protoplanetary disks show that carbon fractionation proceeds in the surface layer and outer disk where isotope selective photodissociation occurs (Woods and Willacy 2009; Visser et al. 2018).

$\text{HC}^{18}\text{O}^+$  has recently been detected towards the TW Hya disk by ALMA, and a ratio of  $\text{H}^{13}\text{CO}^+/\text{HC}^{18}\text{O}^+ = 8.3 \pm 2.6$  was derived. Considering exchange reactions and the derived  $\text{H}^{13}\text{CO}^+/\text{HC}^{18}\text{O}^+$  ratio,  $^{13}\text{CO}/\text{C}^{18}\text{O} = 8.1 \pm 0.8$  is obtained, which is consistent with the detailed model calculation (Furuya et al. 2022). Oxygen isotope fractionation in the protosolar nebula has been proposed in the context of a possible link to the oxygen isotope anomaly discovered in meteorites (Lyons and Young 2005, see also Section 6). Relatively simple protoplanetary disk chemical models with isotope selective photodissociation of CO and isotope exchange reactions have been constructed, mainly focusing on fractionation of the CO isotopologues in order to help derive disk gas masses observationally (Miotello et al. 2014, 2016). Further investigation of carbon and oxygen isotope fractionation in various molecules in disks will help provide insight into the possible link between materials in planet forming regions and those in the solar system.

### 3.4. Future prospects to link planet forming regions to the solar system

In order to link planet forming regions to the solar system, we need to understand how observable gas-phase compositions in the disk surface are linked to the ice compo-

sition near the disk midplane (*i.e.* the building blocks of planetesimals and then objects in planetary systems). Theoretically, constructing models of gas-phase and grain surface isotope chemistry together with turbulent motion and dust dynamics (e.g., Krijt et al. 2020) will improve our understanding. Observations of isotopologues which are just evaporated from ice and preserve the ice isotopic ratios, for example, in the disks of FU Ori-type young outbursting objects (e.g., Lee et al. 2019), disks with strong dust concentrations (e.g., van der Marel et al. 2021; Booth et al. 2021), and potentially in debris disks (e.g., Kóspál et al. 2013; Moór et al. 2017; Higuchi et al. 2019), will also be key. Searching for potential correlations among different isotopes (e.g., Guzmán et al. 2017; Marty 2012; Alexander et al. 2012a) will also be useful for further understanding the link.

## 4. COMETS

Comets are composed of ice and dust accreted during the epoch of planet formation, and are believed to have been subject to relatively little chemical alteration since that time (Mumma and Charnley 2011). Their study therefore provides a unique window into the isotopic composition of material from the early solar system, including volatiles (ice) from the protosolar disk and prior interstellar cloud, as well as refractory material (dust) that may have undergone significant thermal processing closer to the sun. The volatile inventory of comets is dominated by  $\text{H}_2\text{O}$ ,  $\text{CO}_2$  and CO ices, complemented by similar abundances of organic molecules and sulphur-bearing species to those found in interstellar ices, as well as in the warm, protostellar gas where ice mantles have been evaporated.

### 4.1. Carbon isotopes in the pre-Rosetta era

Isotopic studies of comets, date back to the first measurement of the  $^{12}\text{C}/^{13}\text{C}$  ratio in  $\text{C}_2$ , observed in optical emission from the coma of Ikeya 1963 I (Stawikowski and Greenstein 1964). Observations of  $^{13}\text{CC}$  and  $\text{C}_2$  in a number of subsequent apparitions revealed an average  $^{12}\text{C}/^{13}\text{C}$  ratio of  $90 \pm 8$  (error weighted mean with associated one-sigma uncertainty; see review by Bockelée-Morvan et al. 2015), which is fully consistent (within errors) with the Solar and terrestrial carbon isotopic abundances. Cometary CN was found to suffer from less spectral line blending than  $\text{C}_2$ , and a mean value of  $^{12}\text{C}/^{13}\text{C} = 91 \pm 4$  was derived from CN in a diverse sample of 21 comets by Manfroid et al. (2009).

### 4.2. Deuteration of cometary volatiles

The power of isotopic measurements for elucidating cometary origins became more apparent with the D/H measurement in comet 1P/Halley’s water coma by the Giotto spacecraft ( $(3.1 \pm 0.3) \times 10^{-4}$ ; (Eberhardt et al. 1995), later revised to  $(2.1 \pm 0.3) \times 10^{-4}$ ; Brown et al. 2012). These mass spectrometry measurements indicated a significant deuterium enrichment in cometary ice compared

with the primordial (Solar) value of  $2.1 \times 10^{-5}$ . Detections of D/H have now been published for 11 different comets using in situ mass spectrometry, ground-based optical spectroscopy of OD/OH and mm/sub-mm/IR measurements of HDO/H<sub>2</sub>O/H<sub>2</sub><sup>18</sup>O, revealing a distribution of values  $[D/H]_{H_2O}$  in the range  $(1.0\text{--}8.1) \times 10^{-4}$ , with an error-weighted mean of  $(2.1 \pm 0.1) \times 10^{-4}$ . This includes the value of  $(5.3 \pm 0.7) \times 10^{-4}$  measured by the ROSINA mass spectrometer in comet 67P (Altwegg et al. 2015), as well as the recently-obtained value  $(1.6 \pm 0.7) \times 10^{-4}$  in comet 46P using the Stratospheric Observatory for Infrared Astronomy (SOFIA; Lis et al. 2019). A summary of the cometary D/H measurements obtained to-date is shown in Figure 1.

While there appears to be genuine diversity in  $[D/H]_{H_2O}$  across the comet population, the currently available statistics are relatively noisy, and constitute a sensitivity-limited sample. Some upper limits or non-detections are likely to have been unreported, and upper limits are not included in our average value, so the error-weighted mean is therefore biased in the direction of the (larger) reported D/H measurements. More accurate statistics from future observations will be very useful to confirm the true distribution (and average D/H ratio) in comets. For the time being however, it is reasonable to consider typical comets as somewhat enriched in deuterium relative to VSMOW — 67P being the most significantly enriched, at  $(2.9\text{--}3.8) \times$  VSMOW.

There is no strong evidence that different D/H values occur in comets from different dynamical reservoirs (originating from different parts of the protoplanetary disk). However, a trend for decreasing D/H as a function of active surface fraction (the ratio of sublimating area to the total surface area of the nucleus) observed by Lis et al. (2019) could be interpreted as resulting from the presence of two isotopically distinct ice reservoirs in the nucleus: one reservoir in the relatively ice-poor material residing close to the surface of the nucleus (preferentially released in lower-activity comets), and a different, lower D/H reservoir in the ice-rich grains, which can contribute strongly to the active (sublimating) surface area (see also Fulle 2021). Alternative explanations for the trend observed by Lis et al. (2019) include the possibility of sublimation-dependent deuterium fractionation, for example, as observed in the laboratory by Lécuyer et al. (2017) (albeit at a relatively low level), or as a result of non-steady-state deuterium enrichment of the coma, as predicted by the sublimation model of Podolak et al. (2002).

The detection of a surprisingly large D<sub>2</sub>O abundance in comet 67P by Rosetta (with  $D_2O/HDO = (1.8 \pm 0.9) \times 10^{-2}$ ) provided crucial new constraints on the origins of cometary H<sub>2</sub>O, beyond what can be inferred from the HDO/H<sub>2</sub>O ratio alone (Altwegg et al. 2019). The Furuya et al. (2017) model for a collapsing, infalling, irradiated protostellar envelope generates insufficient deuteration to reproduce the 67P D<sub>2</sub>O/HDO ratio. However, similar values of D<sub>2</sub>O and HDO enrichment to those found in 67P readily occur in the cold interstellar phase preceding star formation. The doubly-deuterated isotopologue thus provides a strong in-

dicator for the interstellar heritage of cometary water.

Another important result from the Rosetta mission was the first detection of deuterated CH<sub>3</sub>OH in comets, with a relatively large abundance ratio  $(CH_2DOH + CH_3OD)/CH_3OH = (5.5 \pm 0.5) \times 10^{-2}$  measured in the coma of 67P (Drozdovskaya et al. 2021). The similarity between this value and the D<sub>2</sub>O/HDO ratio, combined with the theoretical result that deuteration of both H<sub>2</sub>O and CH<sub>3</sub>OH proceeds in interstellar ices via D-H atom-exchange reactions, implies that deuterated methanol formed relatively late in the protosolar cloud core (prior to collapse), when gas-phase atomic D was more abundant, but while the temperatures were still low enough to preserve significant amounts of CO in the ice for CH<sub>3</sub>OH production. The relatively lower ratios of HDS/H<sub>2</sub>S and NH<sub>2</sub>D/NH<sub>3</sub> in comet 67P of  $\sim 6 \times 10^{-4}$  and  $\sim 1 \times 10^{-3}$ , respectively (Altwegg et al. 2019), and of DCN/HCN ( $2.3 \times 10^{-3}$ ) in comet O1 (Hale-Bopp) are consistent with deuteration occurring in these molecules at a somewhat earlier (prestellar) epoch (Drozdovskaya et al. 2021), when atomic D was less abundant.

### 4.3. Nitrogen fractionation in comets

Observations of nitrogen fractionation in comets were reviewed by Bockelée-Morvan et al. (2015) and Hily-Blant et al. (2017), who reported a weighted average <sup>14</sup>N/<sup>15</sup>N ratio of  $144 \pm 3$  in HCN, CN and NH<sub>2</sub> (from 31 comets). Cometary ices observed to-date show a ubiquitous enrichment in <sup>15</sup>N with respect to the bulk of the material from which the solar system formed (represented by the Jovian and solar wind-derived values: <sup>14</sup>N/<sup>15</sup>N  $\approx 440$ ; Owen et al. 2001; Marty et al. 2011), as well as with respect to the terrestrial value of 272 (Junk and Svec 1958). There is no strong evidence for diversity in individual <sup>14</sup>N/<sup>15</sup>N values across the comet population (disk <sup>14</sup>N/<sup>15</sup>N ratios are also quite consistent, with values  $\sim 100\text{--}300$ ), implying a uniformity in the nitrogen fractionation processes occurring in the outer parts of protoplanetary disks, where comets are believed to have accreted. ROSINA mass spectrometry of NH<sub>3</sub> and NO in the 67P coma provided in situ confirmation of this trend (Altwegg et al. 2019). Surprisingly, a consistent isotopic fingerprint was also found in 67P’s molecular nitrogen, which had <sup>14</sup>N/<sup>15</sup>N  $\sim 130 \pm 30$ . Considering N<sub>2</sub> is believed to be a major reservoir of nitrogen in protoplanetary disks (e.g., Walsh et al. 2015), and the giant planets (representative of that reservoir; see Section 6) show a lack of <sup>15</sup>N fractionation, the molecular nitrogen observed in comet 67P is unlikely to have been directly inherited from primordial (or interstellar) N<sub>2</sub> in the disk, and must originate from more isotopically-processed nitrogenous material. Overall, the nitrogen isotopes in 67P are consistent with accretion from a relatively uniformly-fractionated ice reservoir, most likely dominated by the <sup>15</sup>N-enrichment resulting from isotope-selective photodissociation of N<sub>2</sub> (see Section 2.4).

#### 4.4. Oxygen fractionation in cometary volatiles

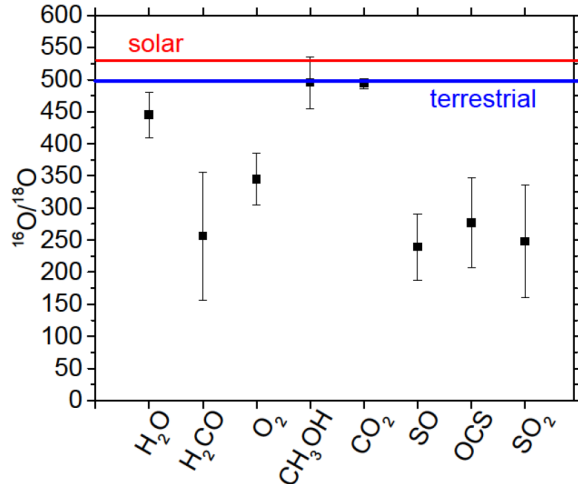


Fig. 5.—  $^{16}\text{O}/^{18}\text{O}$  ratios for eight molecules observed using Rosetta mass spectrometry of the comet 67P coma. Solar and terrestrial baseline values are shown in red and blue, respectively. Figure reproduced from *Altwegg et al. (2020)*.

Prior to the Rosetta mission to comet 67P, evidence for significant oxygen fractionation in comets was scarce, particularly when considering the weighted-mean  $^{16}\text{O}/^{18}\text{O}$  ratio of  $495 \pm 19$  (at  $1\sigma$  confidence) from the 9 measurements compiled by *Bockelée-Morvan et al. (2015)*, which is consistent with the terrestrial value of 499 and close to the solar value of 530; *McKeegan et al. 2011*. Rosetta measured  $\text{H}_2\text{O}/\text{H}_2^{18}\text{O} = 445 \pm 35$  in 67P (*Schroeder I et al. 2019*), corresponding to a modest enhancement in  $^{18}\text{O}$  compared with terrestrial and solar wind values. Comet 67P's  $\text{CO}_2$  (the next most abundant ice in the nucleus) on the other hand, shows no evidence for oxygen fractionation (with  $^{16}\text{O}/^{18}\text{O} = 494 \pm 8$ ). These oxygen isotope results are consistent with chemical models incorporating isotope-selective photodissociation of CO in the protosolar nebula. An  $^{18}\text{O}$  enrichment of 5-20% is predicted in  $\text{H}_2\text{O}$  by the models of *Lyons and Young (2005)* and *Lee et al. (2008)* as a result of preferential photodissociation of  $\text{C}^{18}\text{O}$  compared with CO. On the other hand,  $\text{CO}_2$  forms from O-atom addition to the dominant CO isotopologue, which is less efficiently dissociated than the minor isotopologues due to self-shielding in the dense nebular gas.

The high sensitivity and resolution of Rosetta's ROSINA mass spectrometer afforded unprecedented precision in the  $^{16}\text{O}/^{18}\text{O}$  ratios for several previously unmeasured molecules in comets (*Altwegg et al. 2020*).  $\text{O}_2$ ,  $\text{H}_2\text{CO}$ , and the sulphur-bearing species SO,  $\text{SO}_2$  and OCS all show strong ( $\sim$  factor of two) enrichments in  $^{18}\text{O}$  compared with the terrestrial value (see Figure 5), whereas  $\text{CH}_3\text{OH}$  shows a ratio consistent with terrestrial. Similarity of the  $^{16}\text{O}/^{18}\text{O}$  ratios in  $\text{CO}_2$  and  $\text{CH}_3\text{OH}$  is expected based on their theorized common origin from atom-addition to CO on grain

surfaces. By contrast, the discrepancy in  $^{16}\text{O}/^{18}\text{O}$  for  $\text{H}_2\text{CO}$  implies a different origin for this molecule; *i.e.* CO cannot be its main chemical precursor. This is also implied by the strong ( $\sim$  factor of two) enrichment in the  $^{13}\text{C}$  fraction of  $\text{H}_2\text{CO}$ , which is not observed in CO.  $\text{CO}_2$ ,  $\text{CH}_3\text{OH}$  and  $\text{C}_2\text{H}_6$  also show a lack of any significant  $^{13}\text{C}$  enrichment (*Hässig et al. 2017; Altwegg et al. 2020*). Observations of CO,  $\text{H}_2\text{CO}$  and  $\text{CH}_3\text{OH}$  isotopologues by in the DR21 (OH) high-mass protostellar core show a similar trend to 67P, with  $\text{H}_2\text{CO}$  significantly enriched in  $^{13}\text{C}$  compared with CO and  $\text{CH}_3\text{OH}$ . Based on its unusual spatial distribution, cometary  $\text{H}_2\text{CO}$  is believed to originate (at least in part) from the degradation of organic-rich dust or macromolecular material in the coma (*Cottin and Fray 2008; Cordiner et al. 2014*), so the unusual isotopic composition of  $\text{H}_2\text{CO}$  in 67P could be inherited from organic refractories. Future observations of  $\text{H}_2\text{CO}$  isotopologues in comets with confirmed extended sources of  $\text{H}_2\text{CO}$  will enable further exploration of this hypothesis.

The comet 67P results showing significant  $^{18}\text{O}$  enrichment in  $\text{O}_2$ , SO,  $\text{SO}_2$  and OCS, along with modest enrichment in  $\text{H}_2\text{O}$  and negligible enrichment in  $\text{CH}_3\text{OH}$  can be explained as a result of isotopic exchange reactions involving atomic  $^{18}\text{O}$  in low temperature, interstellar gas (*Loison et al. 2019b*) (also see Section 2.2). Similar  $^{18}\text{O}$ -exchange reactions are also expected to occur in the cold gas in the outer regions of the protosolar disk (Section 3), so a collapsing cloud + disk model would be required for a more complete interpretation of these ratios. The origin of the  $^{18}\text{O}$  enrichment in  $\text{H}_2\text{CO}$  is less clear, but implies the presence of a latent reservoir of isotopically enriched precursor material, resulting from an unknown fractionation pathway.

#### 4.5. Isotopic composition of cometary dust and refractories

Compositional measurements of the non-volatile component of cometary solids (including dust particles, minerals and refractory solids) are much more challenging than for gas measurements, resulting in a paucity of isotopic measurements compared with the cometary ices. The pioneering Stardust mission to comet 81P/Wild 2 in 2006 brought back coma dust samples to Earth for analysis in the laboratory, allowing individual grains (and their sub-components) to be examined in detail, thus revolutionizing our understanding of the composition of cometary refractories. As summarized by *Bockelée-Morvan et al. (2015)*, the bulk of the material analyzed was surprisingly rich in high-temperature minerals such as crystalline silicates, and conversely, relatively poor in organic material compared with carbonaceous chondrite meteorites. This may be due to loss of the non-refractory material due to heating during sample collection. The Stardust samples showed a range of deuterium enrichments from approximately terrestrial up to  $\sim 3 \times$  VSMOW (*McKeegan et al. 2006*).  $^{13}\text{C}$  was found to be slightly depleted ( $\delta^{13}\text{C} = -20$  to  $-50$  per mil, where  $\delta X$  is the fractional enrichment of isotope X relative to a terres-

trial standard; see e.g. *Füri and Marty* 2015). The  $^{15}\text{N}/^{14}\text{N}$  ratio is similar to the terrestrial value, but with some outliers ( $\delta^{15}\text{N} = +100$  to  $+500$  per mil), and in small-scale isotopic ‘hotspots’, the maximum  $\delta^{15}\text{N}$  was  $\approx +1300$  per mil. Minor depletions were found in  $^{18}\text{O}$ , consistent with chondritic material. The overall dust grain isotopic composition in comet Wild 2 is similar to carbonaceous chondrite meteorites — *i.e.* significantly enriched in D and N compared with primordial values, and broadly similar to the terrestrial average (albeit with some significant  $^{15}\text{N}$  and D enrichments); see Section 5.

*Paquette et al.* (2021) presented the first D/H measurements in the organic refractory component of cometary dust particles, based on in situ analysis by the Rosetta COSIMA instrument at comet 67P. The D/H ratio is an order of magnitude larger than VSMOW, and agrees (within errors) with the heavily deuterium-enriched DCN/HCN value found in comet Hale-Bopp (*Meier et al.* 1998). Intermediate between  $\text{H}_2\text{O}$  and  $\text{CH}_3\text{OH}$ , the moderately-high D/H ratio in carbon-rich cometary dust implies an origin from organic matter synthesized (at least, in part), in the cold, dense ISM. More observations of deuterated organic molecules in comets, and at various stages in the chemical evolution from interstellar cloud to protoplanetary disk, will be crucial for understanding the complex history of refractory carbon in cometary dust samples.

#### 4.6. Towards a complete understanding of cometary isotopic signatures

Based on the isotopic ratios of hydrogen, carbon, nitrogen and oxygen, a reasonably consistent picture emerges regarding the origins of cometary ices in cold ( $\sim 10$ – $30$  K), dense, interstellar/protostellar gas, as a combined result of gas phase and grain-surface chemistry. While some reprocessing of interstellar ices is expected in the protosolar accretion disk (and during the passage of interstellar matter into the disk), strong deuterium enrichment in the disk may be inefficient (*Cleeves et al.* 2014; *Furuya et al.* 2017). The physical, chemical and dynamical complexity of the comet-forming environment (see *Estrada et al.* 2016, *Eistrup et al.* 2019 and *Dones et al.* 2015, respectively), together with incomplete information on the state of the protosolar disk at the time of planetesimal formation precludes exact modeling of the cometary accretion process. Nevertheless, a reasonable (at least qualitative) understanding has been achieved regarding the origin of the majority of the observed cometary isotope ratios.

### 5. METEORITES/ASTEROIDS

#### 5.1. Background

The chondritic meteorites are all formed from three basic components: chondrules, refractory inclusions (such as Ca-Al-rich inclusions or CAIs), and matrix (*Scott and Krot* 2014). Chondrules and inclusions formed at high temperatures ( $\sim 1500$ – $2100$  K) in the solar nebula. The fine-grained matrix cements the meteorites and is a mixture of materials

that were thermally processed in the solar nebula (e.g., crystalline silicates), as well as lesser amounts of materials like organic matter and presolar circumstellar grains that were not. Based on their chemical, isotopic and physical properties, the chondritic meteorites have been divided into four classes (ordinary, carbonaceous, enstatite and Rumuruti), and subdivided into a number of groups (ordinary - H, L, LL; carbonaceous - CI, CM, CV, CO, CK, CR, CB, CH; enstatite - EH, EL). Each chondrite group is assumed to have come from a separate asteroidal parent body, although it is possible that there are multiple parent bodies with very similar compositions/properties.

The chondrites formed between  $\sim 2$  Ma and  $\sim 4$  Ma after CAIs (the oldest dated solar system objects). They accreted as unconsolidated ‘sediments’, but lithification processes in their asteroidal parent bodies produced rocks that were strong enough to survive impact excavation and atmospheric entry. This lithification was driven by internal heating due to the decay of  $^{26}\text{Al}$  ( $t_{1/2} \sim 0.7$  Ma). Those asteroids that formed at  $\sim 2$  Ma (ordinary, Rumuruti, enstatite, CK) did not quite get hot enough in their centers to start melting, while heating near their surfaces was relatively mild. For these meteorites, their lithification was predominantly driven by heat (thermal metamorphism) and the extent of their modification will have varied with their depth in their parent bodies. It should be emphasized that, except for the enstatite chondrites, there is clear evidence that they accreted ices, but most experienced high enough peak temperatures to ultimately drive off any water. Parent bodies that formed between 3–4 Ma (e.g., CI, CM, CR) would have had enough  $^{26}\text{Al}$  to melt water-ice and drive reactions that generated hydrous minerals, carbonates, and Fe,Ni-oxides, but generally probably did not reach temperatures above  $\sim 420$  K ( $\sim 150$  °C) and can exhibit a wide range in extents of alteration. If planetesimals formed after  $\sim 4$  Ma, there would not have been enough  $^{26}\text{Al}$  to even melt ice, although impacts could potentially accomplish this at least briefly and locally. Thus, these bodies are unlikely to be the sources of meteorites, but could be sources of some interplanetary dust.

Recently, it has become apparent that in the early solar system the asteroid belt was probably a dynamical dumping ground for planetesimals that formed over a wide range of orbital distances from the Sun and were scattered there by the giant planets. Chondrites, as well as iron and achondrite meteorites from earlier formed differentiated planetesimals, are now often classified as carbonaceous and non-carbonaceous (the latter including Earth, Moon and Mars) based on small but systematic isotopic variations in multiple elements (e.g., Ca, Ti, Cr, Mo, Ru) that are nucleosynthetic in origin (*Warren* 2011). The association of the non-carbonaceous group with Earth and Mars, as well as the need to keep the carbonaceous and non-carbonaceous groups physically separated, has led to the suggestion that the non-carbonaceous group formed inside of Jupiter’s orbit and the carbonaceous group outside its orbit (*Budde et al.* 2016; *Kruijer et al.* 2017; *Warren* 2011).

## 5.2. Carbon and Nitrogen isotopes in meteoritic organics

In primitive chondritic meteorites, C and N are primarily carried by organic material, with lesser amounts of C in carbonate minerals. On the other hand, H is found predominantly in hydrous minerals (clays, etc.) as OH and H<sub>2</sub>O, with only roughly 10 % in organic material. Oxygen is distributed between the anhydrous silicates/oxides that were accreted from the nebula, the OH/H<sub>2</sub>O in hydrous silicates, and products of Fe,Ni-metal and -sulfide oxidation by H<sub>2</sub>O. In more thermally metamorphosed samples, dehydration and mineral reactions have erased most signs of any early aqueous alteration, but its influence will still be recorded in their bulk O isotopes and FeO contents. The organics, on the other hand, were destroyed by metamorphism. In most chondrites, the organics were oxidized and lost from all but the least heated samples. In the highly reduced enstatite chondrites, the organics became increasingly graphitized with the loss of H, N and O. Some N may be retained in minerals like TiN, Si<sub>3</sub>N<sub>4</sub>, and Si<sub>2</sub>N<sub>2</sub>O, although there is debate about whether these minerals are metamorphic or formed in the solar nebula. The extent to which aqueous alteration altered organics is even more controversial.

The C isotopic compositions of bulk chondrites fall in a relatively restricted range of  $^{12}\text{C}/^{13}\text{C} \approx 87.5\text{--}91.0$ , the variations largely reflecting differing relative abundances of the more abundant ( $^{12}\text{C}/^{13}\text{C} \approx 89\text{--}92$ ) organic material *Alexander et al.* (2007), and the less abundant carbonate ( $^{12}\text{C}/^{13}\text{C} \approx 82\text{--}90$ ) (*Alexander et al.* 2015; *Fujiya et al.* 2015; *Grady et al.* 1988; *Telus et al.* 2019; *Vacher et al.* 2017). The origin of the carbonate C has yet to be established, but may have been volatile carbonaceous species (e.g., CO<sub>2</sub>, CO, CH<sub>4</sub>) trapped in the accreted ices. In bulk the carbonate C isotopic compositions are quite variable even within a group (e.g.,  $^{12}\text{C}/^{13}\text{C} \approx 82.9\text{--}88.7$  in CMs), and vary considerably more from grain to grain in a meteorite. These variations suggest that the carbonate C isotopic compositions probably reflect the evolving conditions (i.e., temperature and gas/fluid compositions) during precipitation more than the source composition(s).

The bulk of the C and N in chondrites is present in organic material, most of which cannot be extracted with solvents (*Alexander et al.* 2017b). This insoluble material is distributed throughout the matrix in mostly sub-micron grains that show no obvious spatial relationship to any minerals. Larger grains seem to be aggregates of smaller grains that have collected in veins, perhaps as the result of fluid flow. For reasons that are unclear but may be related to their small grain size, efficient isolation of this insoluble material from chondrites has proved to be extremely difficult, with yields that are typically ~50 %. What is isolated is usually referred to as insoluble organic material (IOM). In terms of H/C ratio, aromaticity and isotopic composition (all indicators of extent of thermal/hydrothermal processing), the most primitive IOM is found in the CR chondrites, the youngest chon-

drates that probably saw the lowest peak alteration temperatures. The CR IOM has a bulk elemental composition, relative to 100 Cs, of C<sub>100</sub>H<sub>75–79</sub>O<sub>11–17</sub>N<sub>3–4</sub>S<sub>1–3</sub> (*Alexander et al.* 2007), which is not very different to the composition of Halley CHON particles (C<sub>100</sub>H<sub>80</sub>O<sub>20</sub>N<sub>4</sub>S<sub>2</sub> (*Kissel and Krueger* 1987)) and the refractory carbonaceous dust in comet 67P/Churyumov-Gerasimenko (C<sub>100</sub>H<sub>104</sub>N<sub>3.5</sub> (*Fray et al.* 2017; *Isnard et al.* 2019), for which O and S were not measured). The CRs also generally have the most isotopically anomalous IOM with bulk D/H  $\approx 5.5\text{--}6.4 \times 10^{-4}$  and  $^{14}\text{N}/^{15}\text{N} \approx 221\text{--}237$ , although a few ungrouped chondrites are more anomalous with bulk IOM D/H ratios as high as  $7.0 \times 10^{-4}$  and  $^{14}\text{N}/^{15}\text{N}$  ratios as low as 192. These IOM H isotopic compositions are not as D-rich as the refractory carbonaceous material in 67P (D/H =  $1.57 \pm 0.54 \times 10^{-3}$  (*Paquette et al.* 2021)), but they and the elemental compositions hint at a genetic link, with the material in 67P having experienced less modification in the nebula and/or the comet than the IOM in the chondrites. When analyzed at micron to sub-micron scales, the CR IOM contains a few percent of isotopic hotspots with D/H ratios up to  $6.4 \times 10^{-3}$  and  $^{14}\text{N}/^{15}\text{N}$  ratios as low as 68. These hotspots seem to be associated with individual grains, but there is no straightforward correlation between the D and  $^{15}\text{N}$  enrichments (*Busemann et al.* 2006; *Hashiguchi et al.* 2015).

IOM has been isolated from at least some members of all chondrite groups except the Rumuruti and CK chondrites, which are too metamorphosed to have preserved much, if any IOM. The IOM in the non-CR chondrite groups is generally not as isotopically anomalous and has lower H/C ratios than the CR IOM that, if all IOM had the same or similar precursors, are an indication of heating. This heating most likely occurred in their parent bodies, but some heating in the disk prior to accretion cannot be ruled out. Interplanetary dust particles also contain significant amounts of refractory, insoluble organic C (*Schramm et al.* 1989; *Thomas et al.* 1993). In the anhydrous chondritic porous (CP-) IDPs, which are likely to have come from comets, most or all the H should be associated with organic material. Measurements of their H isotopic compositions are generally not as anomalous as the IOM in the CRs, for instance, when analyzed at similar scales (*Messenger et al.* 2003). However, like the IOM, there are hotspots that can have similarly extreme D and  $^{15}\text{N}$  enrichments. The less anomalous isotopic compositions of CP-IDPs could simply be the result of atmospheric entry heating driving off the more thermally labile and isotopically anomalous functional groups.

Although not as abundant as the IOM, there are very complex suites of solvent-soluble organics in the primitive chondrites (*Glavin et al.* 2018; *Schmitt-Kopplin et al.* 2010). The absolute and relative abundances of the different molecules differ from meteorite to meteorite in ways that are still poorly understood, but they seem to be a function of the extent of aqueous alteration. These variations indicate that the aqueous chemistry in the meteorites was quite dynamic, and what is present now is almost certainly

not the same as what was accreted (*Danger et al.* 2021). The best studied family of soluble molecules are the amino acids. They also tend to be the most isotopically anomalous, with  $D/H \approx 1.65\text{-}12.6 \times 10^{-4}$ ,  $^{14}\text{N}/^{15}\text{N} \approx 205\text{-}269$ ,  $^{12}\text{C}/^{13}\text{C} \approx 84.5\text{-}91.0$  (*Elsila et al.* 2012; *Martins and Sephton* 2009), albeit with considerable variability within and between meteorites. The most abundant amino acids in the least altered chondrites are the so-called  $\alpha$ -amino acids that are thought to have formed by reaction of simpler ketones and aldehydes with  $\text{NH}_3$  and  $\text{HCN}$  in aqueous solutions (Strecker-cyanohydrin synthesis).

The presence of  $\text{NH}_3$  and  $\text{HCN}$  in the aqueous solutions again is suggestive of there being a link between the ices accreted by the chondrites and those in comets. The simplest amino acid, glycine ( $D/H \approx 2.0\text{-}3.5 \times 10^{-4}$ ,  $^{14}\text{N}/^{15}\text{N} \approx 237\text{-}262$ ,  $^{12}\text{C}/^{13}\text{C} \approx 85.0\text{-}87.8$  (*Elsila et al.* 2012; *Martins and Sephton* 2009), would have formed from formaldehyde with one C added from  $\text{HCN}$  and N added from  $\text{NH}_3$ . The  $^{12}\text{C}/^{13}\text{C}$  ratio of formaldehyde in 67P is  $40 \pm 14$  (*Altwegg et al.* 2020), which is isotopically much heavier than formaldehyde in the Murchison meteorite ( $^{12}\text{C}/^{13}\text{C} \approx 83.4$  (*Simkus et al.* 2019)), or glycine or any other amino acid measured in chondrites. The  $^{14}\text{N}/^{15}\text{N}$  ratios of  $\text{NH}_3$  and  $\text{HCN}$  in comets are very uniform ( $\sim 140$ ) and again much heavier than in glycine in chondrites. Unless  $\text{HCN}$  has a very light  $^{12}\text{C}/^{13}\text{C}$  ratio to compensate for the heavy composition of the formaldehyde and there are as yet unrecognized sources of  $^{15}\text{N}$ -depleted  $\text{NH}_3$  in comets, the glycine isotopic compositions in chondrites point to differences in the nature of the ices accreted by chondrites and primitive comets like 67P.

### 5.3. Hydrogen isotopes in meteoritic water and organics

While the organic material can be very enriched in D, the D/H of the bulk meteorites are much lower. For instance, for the CMs the IOM  $D/H \approx 2.5\text{-}3.4 \times 10^{-4}$ , while the bulk meteorites have  $D/H \approx 1.2\text{-}1.8 \times 10^{-4}$ . The reason for this difference is that the water accreted by the chondrites was isotopically much lighter than the organics. How much lighter can be estimated by plotting D/H vs. C/H for the bulk meteorites in a group that have significant variation in the extents of alteration. In this case, the bulk compositions should produce a linear trend reflecting variable mixing of the H in water (now in clay minerals, etc.) and organics, with projection to  $C/H = 0$  giving an estimate of the D/H of the water and extension of the trend to high C/H passing through the initial bulk D/H of the organics. In this way, *Alexander et al.* (2012b) estimated that the water accreted by the CMs and the CIs had a  $D/H \approx 8.6 \times 10^{-5}$ , and that the initial bulk organic D/H was similar to that of IOM in the CRs (i.e., there has been D/H exchange between water and organics during alteration). The CRs, on the other hand, seem to have accreted more D-rich water with a  $D/H \approx 1.7 \times 10^{-4}$ .

The D/H of the water accreted by the other carbona-

ceous chondrite groups is more difficult to estimate because metamorphism has resulted in at least partial dehydration and modification of the organics. The water D/H ratios in CI, CR, CM and CV chondrites have been estimated by measuring in situ the D/H and C/H ratios of multiple areas  $10\text{-}15 \mu\text{m}$  across of bulk meteorites (*Piani and Marrocchi* 2018; *Piani et al.* 2015, 2018). The estimated D/H ratios of  $1.55 \times 10^{-4}$  for the CIs,  $1.0 \times 10^{-4}$  for the CMs and  $2.38 \times 10^{-4}$  for the CRs are more D-rich than the estimates based on bulk measurements above. The  $D/H \approx 1.4 \times 10^{-4}$  for the CVs is intermediate between the bulk estimates for the CMs/CIs and CRs. If there has been water-organic H isotopic exchange, for instance, the in situ measurements will reflect the current average D/H ratios of the water and organics rather than their initial compositions. However, *Piani et al.* interpret their results as reflecting the accreted water compositions, so that the variations that they observe amongst the CMs imply heterogeneous accretion of at least two isotopically distinct ices. *Piani et al.* (2015) reported possible evidence for even more dramatic H isotopic heterogeneity in ices accreted by the primitive ordinary chondrite Semarkona, with compositions of  $1.5 \times 10^{-4}$  and  $1.8 \times 10^{-3}$ . However, *Shimizu et al.* (2021) have attributed this range to terrestrial contamination and parent body processes (see below).

There are two sources of uncertainty in the estimates of the water D/H. First, the extent of terrestrial contamination by atmospheric water in the samples analyzed by *Alexander et al.* (2012b) have probably been underestimated (*Lee et al.* 2021a; *Vacher et al.* 2020), which will change both the C/H and D/H values. How much this will change the estimates of the water D/H remains to be seen, but it is likely to affect the CRs more than the CMs. Terrestrial contamination will also have effected in situ measurements, but the extent to which contamination has compromised them has also not been quantified. Secondly, it is possible that the D/H of the water was modified during the early stages of aqueous alteration when metal was oxidized (*Alexander et al.* 2010). Reactions such as  $3\text{Fe} + 4\text{H}_2\text{O} = \text{Fe}_3\text{O}_4 + 4\text{H}_2$  would have generated copious amounts of  $\text{H}_2$ . So much  $\text{H}_2$ , in fact, that unless it found ways to escape to space the pore pressure would have exceeded the tensile strength of an asteroid, leading to its catastrophic disruption. At temperatures of  $270\text{-}470 \text{ K}$  ( $0\text{-}200 \text{ }^\circ\text{C}$ ), isotopic exchange between  $\text{H}_2\text{O}$  and  $\text{H}_2$  is relatively facile (*Pester et al.* 2018) and there is a very large isotopic fractionation with the  $\text{H}_2$  being very depleted in D. On Earth, for instance,  $\text{H}_2$  with  $D/H \approx 3.1\text{-}6.2 \times 10^{-5}$  has been found escaping areas undergoing low temperature serpentinization (aqueous alteration that is quite similar to what meteorite experienced). Continuous loss of such D-poor  $\text{H}_2$  will result in the remaining water becoming increasingly D-rich, with the degree of D enrichment depending on the alteration temperature and the initial water/metal ratio. Based on the valence state of Fe in the bulk meteorites, estimated current water and initial metal contents, and assumed alteration temperatures of  $270\text{-}470 \text{ K}$  ( $0\text{-}200 \text{ }^\circ\text{C}$ ), *Sutton et al.* (2017) estimated for the CIs

the initial water  $D/H \approx 5.1\text{-}9.0 \times 10^{-5}$ , for the CMs  $D/H \approx 5.1\text{-}7.9 \times 10^{-5}$ , and for the CRs  $D/H \approx 7.4\text{-}14.7 \times 10^{-5}$ .

Whether one uses the initial estimates or the valence corrected ones, most or all of the CI-CM-CR water  $D/H$  ratios fall between the terrestrial and solar ratios. These are significantly lower than in almost all measured comets. Perhaps the simplest explanation for the range of water  $D/H$  ratios in comets and carbonaceous chondrites is that they reflect variable mixtures of interstellar water and water that re-equilibrated with  $H_2$  at high temperatures in the disk (Cleeves et al. 2016; Horner et al. 2007; Yang et al. 2013). If correct, then the carbonaceous chondrites accreted small but significant amounts of interstellar ices, which would be qualitatively consistent with the presence of presolar circumstellar grains in these chondrites and also might point to an ultimately interstellar origin for their organic matter (Alexander et al. 2017a).

The H isotopic fractionation associated with metal oxidation is likely to have had an even bigger effect in the ordinary and Rumuruti chondrites in which water/metal ratios were much lower than in the three carbonaceous groups. In Semarkona (LL3.0), the least metamorphosed ordinary chondrite, the bulk water  $D/H$  is estimated to be  $2.8\text{-}3.4 \times 10^{-4}$  (Alexander et al. 2012b), and hydrous minerals in one Rumurutiite have  $D/H \approx 7.3 \pm 0.1 \times 10^{-4}$  (McCanta et al. 2008). If the D enrichments are the result of parent body processes, Sutton et al. (2017) estimated that Semarkona's initial water  $D/H \approx 7.4\text{-}18.0 \times 10^{-5}$ , which overlaps, within the large uncertainties, with the initial water  $D/H$  estimates for the carbonaceous chondrites. If the high water  $D/H$  ratios in ordinary and Rumuruti chondrites, which are comparable to the most D-rich comets, are not the result of parent body process, they accreted a higher fraction of interstellar water than comets and carbonaceous chondrites. This would be surprising given that the ordinary and Rumuruti parent bodies formed in the inner solar system relatively early when the ambient nebula temperatures are expected to have been higher than in the formation regions of comets and carbonaceous chondrites in the outer solar system.

#### 5.4. Oxygen isotopes in meteorites

To first order, the range of O isotopic compositions in solar system materials reflect variations in  $^{16}O$  relative to  $^{17,18}O$  (Figure 7). These so-called mass independent isotopic variations are quite different to the mass dependent isotopic variations that are produced by typical physical and chemical processes in which the relative change in the  $^{16}O/^{17}O$  ratio is roughly half that of the  $^{16}O/^{18}O$  ratio. Another striking feature of most solar system materials, is that their O isotopic compositions fall relatively close to that of the Earth ( $^{16}O/^{18}O=498.7$ ,  $^{16}O/^{17}O=2732$ ) and are significantly more  $^{16}O$ -poor than the solar O isotopic composition ( $^{16}O/^{18}O=530$ ,  $^{16}O/^{17}O=2798$ ) (Fujimoto et al. 2009; McKeegan et al. 2011; Yurimoto et al. 2008). This is true even for CP-IDPs that may come

from comets (Nakashima et al. 2012a; Starkey et al. 2014; Starkey and Franchi 2013) and crystalline silicates returned from comet Wild 2 (McKeegan et al. 2006; Nakamura et al. 2008; Nakashima et al. 2012b). The only objects whose O isotopic compositions approach those of the solar composition are refractory inclusions (Krot et al. 2020; Yurimoto et al. 2008), which are rare in Wild 2 dust and CP-IDPs. Only one object has been found with an O isotopic composition ( $^{16}O/^{18}O=539$ ,  $^{16}O/^{17}O=2846$ ) that is more  $^{16}O$ -rich than solar (Kobayashi et al. 2003).

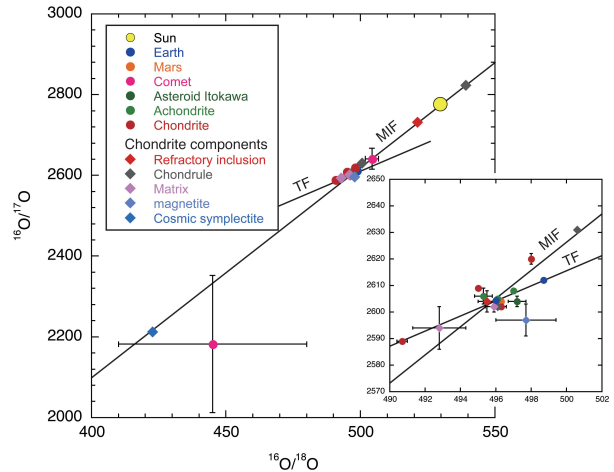


Fig. 6.— The variations in  $^{16}O/^{17}O$  and  $^{16}O/^{18}O$  ratios amongst selected solar system materials. TF is the terrestrial mass fractionation line. MIF is the mass independent fractionation line resulting from the fractionation of  $^{16}O$  from  $^{17}O$  and  $^{18}O$ .

The generally accepted mechanism for producing the mass independent O isotopic variations is by self-shielding during UV dissociation of CO (Section 2.3) that produces  $^{17,18}O$ -rich water and  $^{16}O$ -rich CO. To date, the most extreme  $^{17,18}O$ -enrichment that has been found in any meteoritic material ( $^{16}O/^{18}O=423$ ,  $^{16}O/^{17}O=2231$ ) is in so-called cosmic symplectite (Sakamoto et al. 2007) and provides some idea of what the O isotopic composition of the water generated by self-shield might have been. The  $^{16}O/^{18}O$  ratio of the cosmic symplectite is similar to that of the water in comet 67P (Section 4.4). Because of its volatility and the fact that it is relatively unreactive, to date it has not been possible to directly constrain the O isotopic composition of the CO.

It has been proposed that the CO UV self-shielding took place either in the protosolar molecular cloud (Yurimoto and Kuramoto 2004) or the outer solar system (Lyons and Young 2005), although several arguments seem to favor a molecular cloud origin (Alexander et al. 2017a; Krot et al. 2020). Transferring the  $^{17,18}O$ -enrichments in water to silicates requires high temperatures and separation of the water-ice from the CO. This and the fact that most solar system materials have O isotopic compositions that are fairly close to those of the Earth and Mars, both Yurimoto and Kuramoto



(2004) and *Lyons and Young* (2005) proposed that there was a massive influx of  $^{17,18}\text{O}$ -rich ice from the outer solar system into the inner solar system that changed its bulk composition from solar-like to terrestrial-like. If the carbonaceous chondrites formed beyond the orbit of Jupiter, the O isotopic compositions of most of their components indicates that if such an influx occurred it must have affected some regions of the outer solar system as well. Also, if all silicates with non-solar, more terrestrial-like O isotopic compositions formed inward or somewhat beyond the orbit of Jupiter, this would imply considerable outward radial transport of a large fraction of the material in comets like Wild 2 and the possibly cometary parent bodies of the CP-IDPs.

However, there are two potential mechanisms for producing terrestrial-like O isotopic compositions in silicates anywhere in the solar system if heat sources can be found (e.g., FU Orionis events, impacts and shocks). One mechanism is to simply concentrate silicate dust and ice relative to CO in the gas (*Alexander et al.* 2017a). In this case, the O isotopic composition rapidly asymptotes to the bulk composition of the silicates plus ice, which is terrestrial-like, with increasing (dust+ice)/gas ratio. This scenario would also predict that refractory inclusions formed in regions with very modest (dust+ice)/gas enrichments, relative to solar, a conclusion that others have reached based on the valence states of Ti and V (*Simon et al.* 2007). It also predicts that objects that have O isotopic compositions that are more  $^{16}\text{O}$ -rich than solar should be rare because they would only form in (dust+ice) depleted regions. An alternative mechanism is suggested by experiments that show that amorphous forsterite and enstatite exchange O isotopes with water vapor at relatively low temperatures (e.g., complete isotopic exchange if heated to 500-650 K for the lifetime of the disk), but the less reactive CO does not (*Yamamoto et al.* 2018, 2020). The attraction of this mechanism is that most or all interstellar silicates are amorphous and one would not need to even concentrate the silicate dust and ice relative to the gas.

## 6. PLANETARY ATMOSPHERES

In this section we discuss the complexities in attempting to explain present-day isotopic ratios in planetary atmospheres, the regimes for which we have the most data points across the solar system (meteoritic ratios are discussed in §5). There are two important considerations: (1) The value at time of formation; (2) subsequent enrichment/de-enrichment processes.

For (1) — formation — planets form a middle ground between the protoplanetary disks discussed in §3, and the small icy bodies such as comets discussed in §4. In essence, planets may accrete from both gaseous and solid reservoirs with different molecular constituents and different inherent isotopic ratios due to previous fractionation processes. For example, it is well established that hydrogen exchange occurs leading to D/H in  $\text{H}_2$  (gas phase) being typically much lower than D/H in ices such as  $\text{CH}_4$ ,  $\text{H}_2\text{CO}$  and  $\text{NH}_3$  (Fig. 1)

(*Mousis et al.* 2002). Since different planets accrete different proportions of ice and gas depending on their mass and distance from the star in the proto-planetary disk (e.g. compare Earth to Jupiter) the original bulk isotopic ratios are thus also different. This is the first cause of isotopic ratio variations, and most evident for D/H in planetary atmospheres.

In the case of (2) — processes — planetary atmospheres host many different isotope-selective physical and chemical phenomena, including some not possible for disks or molecular clouds. Important early work on isotopic evolution of planetary atmospheres was performed by Kasting, Hunten and colleagues (*McElroy and Hunten* 1969; *Hunten* 1973, 1982; *Kasting and Pollack* 1983; *Hunten et al.* 1987; *Pepin* 1991). It is now known that many processes act to change atmospheric isotopic ratios, including:

1. Exchange processes (*Thiemens* 1999);
2. Isotope-selective photo-dissociation (*Liang et al.* 2007);
3. Kinetic Isotope Effect (KIE) in chemical reactions, including gas phase (*Pinto et al.* 1986; *Nixon et al.* 2012) and solid formation (*Sebree et al.* 2016);
4. Non-thermal escape processes such as ion pick-up (*Lammer et al.* 2020), where molecules are first ionized and then become attached to the magnetized plasma of the solar wind and escape; and photochemical production of suprathermal ions (*Jakosky et al.* 1994);
5. Other mass-dependent escape processes, including thermal (Jeans) escape (*Hunten* 1973), sputtering (*Johnson* 1990), and possible early hydrodynamic escape (*Hunten et al.* 1987);
6. Other non-escape effects that may fractionate molecules or element onto the surface or into interior, for example condensation (*Montmessin et al.* 2005), dissolution in seas and oceans (*Benson and Krause* 1984), enclathratization in ice matrix (*Hesse and Harrison* 1981), and others.

It is beyond the scope of this review to describe all of these processes in detail – see review by *Lammer et al.* (2018) and references therein. These fractionation processes lead to further variations in D/H and also in  $^{14}\text{N}/^{15}\text{N}$  between the atmospheres of terrestrial planets, although apparently much less in the case of  $^{12}\text{C}/^{13}\text{C}$  and  $^{16}\text{O}/^{18}\text{O}$ .

In the following sections we will review the current understanding of isotopic ratios in H, C, N and O in the planetary atmospheres of the solar system.

### 6.1. Hydrogen isotopes

Hydrogen D/H is the most variable isotopic ratio across the solar system, from  $\sim 2 \times 10^{-5}$  on the giant planets (*Pierel et al.* 2017),  $\sim 4 \times 10^{-5}$  on the ice giants (*Feuchtkrüger*

et al. 2013), to  $\sim 1.5 \times 10^{-4}$  on Titan and Earth (Niemann et al. 2010; Hagemann et al. 1970),  $9 \times 10^{-4}$  on Mars (Webster et al. 2013) and  $1.6 \times 10^{-2}$  on Venus (Donahue et al. 1982).

This variation is explained by two effects. The first sets a primordial difference due to differing gas ( $\text{H}_2$ ) to ice ( $\text{CH}_4$ ,  $\text{H}_2\text{O}$ ,  $\text{NH}_3$ ) ratios, with the gas giants (Jupiter and Saturn) having the highest fractions of gas, the terrestrial planets the lowest values closest to ices, and the ice giants (Neptune, Uranus) having intermediate values. For terrestrial planet atmospheres, differing rates of water photolysis and escape of H vs. D, have led to increasing D/H from Earth (least fractionated) to Mars to Venus (most fractionated) Therefore, it is important to note that the processed isotopic ratios found in these atmospheres may not reflect the primordial or current bulk ratios in the interior.

D/H values on Titan and Enceladus (Niemann et al. 2010; Waite et al. 2009) appear within a factor 2 of terrestrial D/H, and within the cometary range (Bockelée-Morvan et al. 2015), reflecting an icy composition. There is some evidence for fractionation between gases on Titan ( $\text{CH}_4$ ,  $\text{C}_2\text{H}_2$ , HCN and  $\text{H}_2$ ) (Nixon et al. 2012; Coustenis et al. 2008; Molter et al. 2016; Niemann et al. 2010), however error bars are substantial at this stage, and further work is required to definitively say whether for example there are kinetic isotope effects in play. Some results (Lellouch et al. 2001; Pierel et al. 2017) have indicated that the D/H on Saturn may be slightly lower than on Jupiter, contrary to the expected trend. This result is surprising and needs further work to reduce error bars and confirm.

In addition to long-term evolution, D/H in Martian atmospheric water has been found to exhibit spatial and temporal variation due to seasonal effects, as revealed by measurements for from ground-based and spacecraft observations (Villanueva et al. 2015; Alday et al. 2021).

## 6.2. Carbon isotopes

Mars has the only variation of  $^{12}\text{C}/^{13}\text{C}$  that is demonstrably incompatible with a terrestrial value. The  $^{13}\text{C}/^{12}\text{C}$  enrichment of  $+4.6 \pm 0.4 \%$  in the atmosphere (vs terrestrial PBD) (Webster et al. 2013) may be compared with  $-2.5 \pm 0.5 \%$  in the mantle (Wright et al. 1992). This divergence in atmospheric versus geological  $^{12}\text{C}/^{13}\text{C}$  can be explained if the early Martian atmosphere was CO and  $\text{CH}_4$  with little  $\text{CO}_2$ . CO and  $\text{CH}_4$  are depleted in  $^{13}\text{C}$  and escape, while  $^{13}\text{C}$ -rich  $\text{CO}_2$  is incorporated into the surface (Galimov 2000), mostly prior to 3.9 Gya. In addition, CO may preferentially lose  $^{13}\text{C}$  due to less self-shielding (Hu et al. 2015).  $\text{CO}_2$  may also fractionate due to preferential dissociation of  $^{12}\text{CO}_2$  (Schmidt et al. 2013) and so leave  $^{13}\text{C}$ -rich  $\text{CO}_2$  to be incorporated into surface carbonates.

Recent work on carbon isotopes in multiple species on Titan from Cassini and ALMA have shown no strong evidence for fractionation of  $^{12}\text{C}/^{13}\text{C}$  from methane to daughter species such as hydrocarbons, nitriles and  $\text{CO}_x$  species in the atmosphere (Nixon et al. 2008a; Nixon et al. 2012;

Molter et al. 2016; Serigano et al. 2016; Jennings et al. 2008; Nixon et al. 2008b; Jolly et al. 2010; Iino et al. 2021), although error bars are currently larger than in martian measurements so it may be too soon to definitively rule out any fractionation.

## 6.3. Nitrogen isotopes

Nitrogen, in contrast to neighboring elements on the periodic table carbon and oxygen, exhibits strong variations in isotopic ratio throughout the solar system. This indicates that planetary differences in light element isotopic ratios (other than H) were not primordial, since in that case C and O would be expected to show strong differences between bodies, similar to N. Rather, we conclude that N heterogeneity developed later due to fractionation.

Füri and Marty (2015) have argued that there are three distinct reservoirs of nitrogen evident today: the high  $^{14}\text{N}/^{15}\text{N}$  solar and solar-like ratios seen in Jupiter and Saturn of  $\sim 500$ ; the lower values  $\sim 270$  seen in the inner solar system on Venus, Earth and Moon, and Martian rocks; and finally a still-lower reservoir of  $< 200$  seen on Titan and in comets (see Fig. 1).

An outlier is the atmosphere of Mars, with a ratio of  $\sim 170$  (Wong et al. 2013), much lower than recorded in Martian rocks (Mohapatra and Murty 2003). This indicates substantial escape of isotopically light nitrogen early in its history, which must have occurred early in the solar system when solar EUV was higher to cause hydrodynamic escape, due to efficient cooling by  $\text{CO}_2$  at the present day (Lammer et al. 2018). This difference from Earth and Venus may be due to Mars' lower mass and gravity.

Finally, on Titan an enrichment of  $\sim 3$  is seen in  $^{14}\text{N}/^{15}\text{N}$  from the bulk reservoir of  $\text{N}_2$ , to the photochemical products (nitriles) (Marten et al. 2002; Cordiner et al. 2018; Vinatier et al. 2007; Molter et al. 2016; Iino et al. 2020). An explanation has been offered in terms of self-shielding by  $(^{14}\text{N})_2$  against photolysis, while the less abundant  $^{14}\text{N}^{15}\text{N}$  has no such shielding and therefore photolyzed at a higher rate, providing an atomic source of N which is enriched in  $^{15}\text{N}$ , and subsequently incorporated into CN and other nitrogen-bearing molecules (Liang et al. 2007). The recent Titan photochemical model of Vuitton et al. (2019) incorporates updated molecular nitrogen photolysis cross sections, and provides reasonably good agreement with the level of  $^{15}\text{N}$ -enrichment observed by ALMA in HCN,  $\text{HC}_3\text{N}$  and  $\text{CH}_3\text{CN}$ . However, there appears to be a tendency for the model to overestimate the  $^{15}\text{N}$  enrichment in HCN and  $\text{CH}_3\text{CN}$ , which may be a result of incomplete understanding of Titan's complex atmospheric nitrogen chemistry.

## 6.4. Oxygen isotopes

Oxygen  $^{16}\text{O}/^{18}\text{O}$  does not show strong variations in planetary atmospheres, at the levels seen in nitrogen or hydrogen (see Fig. 1). Smaller variations however have been noted in Earth minerals and meteoritic samples, discussed further in §5.4. Further observational astronomy and/or

probes are needed to determine the  $^{16}\text{O}/^{18}\text{O}$  on the giant planets, since measurements are currently lacking for all four of these bodies other than Jupiter, for which the ratio has a factor of two in error bar (Noll *et al.* 1995).

## 7. SUMMARY

Recent high sensitivity astronomical observations, robotic solar system exploration missions, and detailed analysis of meteorites have made it possible to greatly increase the isotopic measurements in star and planet forming regions as well as solar system objects. Meanwhile, recent developments in chemical modeling have contributed to knowledge of the isotopic links from planet forming regions to the solar system.

- Deuterated species are the most well-studied isotopologues, particularly in the context of the origin of water on the Earth. Recent high spatial resolution observations of protoplanetary disks by ALMA together with chemical modelling suggest warm paths of molecular deuteration in the inner parts of disks, in addition to well-known cold paths in the outer disk.
- Deuterium ratios of various molecular species measured in the comet 67P by Rosetta have provided us with new insights. Models have elucidated the formation processes and epochs of the observed molecules. Isotopic ratios in refractory grains in 67P have also been measured, which show a higher deuterium ratio than the primitive IOM found in CR chondrites, despite their similarity in bulk elemental composition.
- Deuterium ratios in water accreted by various types of meteorites are estimated by measuring the decrease of the deuterium ratios in organics due to aqueous alteration, which show significantly lower values than those in comets and even the Earth's ocean. These estimations suggest a decrease of deuterium fractionation of interstellar water at high temperature in the protosolar nebula.
- Deuterium ratios on Titan and Enceladus are similar to those in comets, suggesting an icy origin, while some possible fractionation in different species have been measured with still significant error bars in the Titan atmosphere.
- Oxygen isotopic ratios in meteorites are interpreted to link to isotope-selective photodissociation of CO and formation of heavy water ice in the star and planet forming region. Oxygen isotope ratios measured in various molecules in the comet 67P are consistent with this scenario and theory of molecular formation in the interstellar medium.
- Transfer of oxygen isotopes from water ice to silicate in meteorites is related to the conditions of the protosolar nebula, such as high temperatures, dust+ice-

to-gas ratios, and crystallinity (amorphous vs. crystalline) of silicates.

- Nitrogen fractionation path through isotope selective photodissociation of  $\text{N}_2$  is proposed, which is qualitatively consistent with recent observations in prestellar/protostellar cores and protoplanetary disks, depending on the amount of small dust grains. In order to understand the N fractionation measurements in  $\text{N}_2$  in the comet 67P in this context, further investigation on the origin of  $\text{N}_2$  is needed.
- Nitrogen isotopic ratios have some variation in the solar system objects, partly due to local processes. ALMA observations of nitrogen fractionation in X-CN organics in Titan's atmosphere can be explained by photochemistry, as is the case of irradiated, dense molecular clouds.
- Carbon isotopic ratios are known to be relatively flat among the solar system objects.  $^{12}\text{C}/^{13}\text{C}$  in various molecular species are measured in the comet 67P by Rosetta, and only  $\text{H}_2\text{CO}$  shows strong fractionation, which resembles observations in a high-mass protostellar core, though further confirmation of such an association will be required. Amino acids in meteorites are known to be isotopically anomalous, but the fractionation is generally less significant compared with those found in comets.

There is still a long way to go to fully understand how material evolves from the planet forming region to solar system objects, although there have been significant new findings observationally and theoretically. Future observations of cold and hot gas-phase molecular isotopologues as well as molecular ices in star and planet forming regions will contribute greatly to our understanding. For example, deeper molecular line surveys using ALMA and other facilities, and high dispersion infrared spectroscopy using thirty meter-class large telescopes, together with future solar system exploration missions will give us further insights on the isotopic link. Theoretically, how to treat isotope chemistry of both gas and ice is the key to understanding the link from astronomical observations of gas in the planet forming regions and primordial solid materials in the solar system. Understanding chemical evolution together with dynamical evolution of gas and dust from prestellar/protostellar cores, protosolar nebula to formation of planetesimals and then planets will provide us clues to better understand the origins of solar system objects. Our knowledge of the isotopic links from planet forming regions to the solar system could be potentially expanded to derive information on the origin of exoplanetary systems from future observations of isotope ratios in exoplanetary atmospheres in future.

**Acknowledgments** We acknowledge P. Hily-Blant, K. Altwegg, Y. Kebukawa, M. Hashiguchi, and D. Yamamoto for their valuable inputs to our chapter, and G. Cataldi and Y. Yamato for kindly providing us data of a figure.

## REFERENCES

- Adams F. C., 2010 *ARA&A*, 48, 47.
- Adande G. R. and Ziurys L. M., 2012 *ApJ*, 744, 2, 194.
- Aikawa Y. and Herbst E., 1999 *ApJ*, 526, 1, 314.
- Aikawa Y. and Herbst E., 2001 *A&A*, 371, 1107.
- Aikawa Y. et al., 2018 *ApJ*, 855, 2, 119.
- Albertsson T. et al., 2014 *ApJ*, 784, 1, 39.
- Alday J. et al., 2021 *Nature Astronomy*.
- Alexander C. M. O. et al., 2007 *Geochim. Cosmochim. Acta*, 71, 4380.
- Alexander C. M. O. et al., 2010 *Geochimica et Cosmochimica Acta*, 74, 4417.
- Alexander C. M. O. et al., 2012a *Science*, 337, 6095, 721.
- Alexander C. M. O. et al., 2012b *Science*, 337, 6095, 721.
- Alexander C. M. O. et al., 2015 *Meteoritics & Planetary Science*, 50, 4, 810.
- Alexander C. M. O. et al., 2017a *Meteoritics & Planetary Science*, 52, 9, 1797.
- Alexander C. M. O. et al., 2017b *Chemie der Erde - Geochemistry*, 77, 2, 227.
- Altwegg K. et al., 2015 *Science*, 347, 6220, 1261952.
- Altwegg K. et al., 2017 *Philosophical Transactions of the Royal Society of London Series A*, 375, 2097, 20160253.
- Altwegg K. et al., 2019 *ARA&A*, 57, 113.
- Altwegg K. et al., 2020 *MNRAS*, 498, 4, 5855.
- Ansdell M. et al., 2016 *ApJ*, 828, 1, 46.
- Benson B. B. and Krause Daniel J., 1984 *Limnology and Oceanography*, 29, 3, 620.
- Bergin E. A. et al., 2004 *ApJ*, 612, 2, 921.
- Bergin E. A. et al., 2013 *Nature*, 493, 7434, 644.
- Bergner J. B. et al., 2020 *ApJ*, 898, 2, 97.
- Birnstiel T. et al., 2012 *A&A*, 539, A148.
- Bizzocchi L. et al., 2013 *A&A*, 555, A109.
- Bockelée-Morvan D. et al., 2015 *SSRv*, 197, 1-4, 47.
- Booth A. S. and Ilee J. D., 2020 *MNRAS*, 493, 1, L108.
- Booth A. S. et al., 2019 *A&A*, 629, A75.
- Booth A. S. et al., 2021 *A&A*, 651, L6.
- Brown P. D. and Millar T. J., 1989 *MNRAS*, 237, 661.
- Brown R. H. et al., 2012 *Planet. Space Sci.*, 60, 1, 166.
- Brünken S. et al., 2014 *Nature*, 516, 7530, 219.
- Budde G. et al., 2016 *Earth and Planetary Science Letters*, 454, 293.
- Busemann H. et al., 2006 *Science*, 312, 727.
- Cataldi G. et al., 2021 *The Astrophysical Journal Supplement Series*, 257, 1, 10.
- Cazaux S. et al., 2011 *ApJL*, 741, 2, L34.
- Ceccarelli C. et al., 2014 *Protostars and Planets VI* (H. Beuther, R. S. Klessen, C. P. Dullemond, and T. Henning), p. 859.
- Chakraborty S. et al., 2014 *Proceedings of the National Academy of Sciences*, 111, 41, 14704.
- Chakraborty S. et al., 2016 *The Journal of Chemical Physics*, 145, 11, 114302.
- Chakraborty S. et al., 2018 *Chemical Physics*, 514, 78, energy and Entropy of Change: From Elementary Processes to Biology.
- Chapillon E. et al., 2011 *A&A*, 533, A143.
- Charnley S. B. and Rodgers S. D., 2002 *ApJL*, 569, 2, L133.
- Clayton R. N., 2002 *Nature*, 415, 6874, 860.
- Cleeves L. I. et al., 2014 *Science*, 345, 6204, 1590.
- Cleeves L. I. et al., 2016 *ApJ*, 819, 1, 13.
- Colzi L. et al., 2018 *MNRAS*, 478, 3, 3693.
- Colzi L. et al., 2020 *A&A*, 640, A51.
- Cooper A. M. and Kästner J., 2019 *Journal of Physical Chemistry A*, 123, 42, 9061.
- Cordiner M. A. et al., 2014 *ApJL*, 792, L2.
- Cordiner M. A. et al., 2018 *The Astrophysical Journal*, 859, 1, L15.
- Cottin H. and Fray N., 2008 *Space Sci. Rev.*, 138, 179.
- Coustenis A. et al., 2008 *Icarus*, 197, 2, 539.
- Dalgarno A. and Lepp S., 1984 *ApJL*, 287, L47.
- Danger G. et al., 2021 *Nature Communications*, 12, 3538.
- Daniel F. et al., 2013 *A&A*, 560, A3.
- Donahue T. M. et al., 1982 *Science*, 216, 4546, 630.
- Dones L. et al., 2015 *SSRv*, 197, 1-4, 191.
- Drazkowska J. et al., 2022 *Protostars and Planets VII*.
- Drozdovskaya M. N. et al., 2021 *MNRAS*, 500, 4, 4901.
- Eberhardt P. et al., 1995 *A&A*, 302, 301.
- Eistrup C. et al., 2019 *A&A*, 629, A84.
- Elsila J. E. et al., 2012 *Meteoritics & Planetary Science*, 47, 9, 1517.
- Estrada P. R. et al., 2016 *ApJ*, 818, 2, 200.
- Faure A. et al., 2015 *A&A*, 584, A98.
- Fedoseev G. et al., 2015 *MNRAS*, 446, 1, 449.
- Feuchtgruber H. et al., 2013 *A&A*, 551, A126.
- Flower D. R. et al., 2006 *A&A*, 449, 2, 621.
- Fray N. et al., 2017 *Monthly Notices of the Royal Astronomical Society*, 469, S506.
- Fuchs G. W. et al., 2009 *A&A*, 505, 2, 629.
- Fujimoto K. et al., 2009 *Geochemical Journal*, 43, 5, e11.
- Fujiya W. et al., 2015 *Geochimica et Cosmochimica Acta*, 161, 0, 101.
- Fulle M., 2021 *MNRAS*, 505, 2, 3107.
- Füri E. and Marty B., 2015 *Nature Geoscience*, 8, 7, 515.
- Furuya K. and Aikawa Y., 2018 *ApJ*, 857, 2, 105.
- Furuya K. et al., 2011 *ApJ*, 731, 1, 38.
- Furuya K. et al., 2013 *ApJ*, 779, 1, 11.
- Furuya K. et al., 2015 *A&A*, 584, A124.
- Furuya K. et al., 2016 *A&A*, 586, A127.
- Furuya K. et al., 2017 *A&A*, 599, A40.
- Furuya K. et al., 2022 *arXiv e-prints*, arXiv:2201.00935.
- Galimov E. M., 2000 *Icarus*, 147, 2, 472.
- Giesen T. F. et al., 2020 *A&A*, 633, A120.
- Glavin D. P. et al., 2018 *The origin and evolution of organic matter in carbonaceous chondrites and links to their parent bodies*, book section 3, pp. 205–271, Elsevier.
- Goldsmith P. F. et al., 2000 *ApJL*, 539, 2, L123.
- Grady M. et al., 1988 *Geochimica et Cosmochimica Acta*, 52, 2855.
- Guilloteau S. and Dutrey A., 1994 *A&A*, 291, L23.
- Guilloteau S. et al., 2006 *A&A*, 448, 2, L5.
- Guzmán V. V. et al., 2015 *ApJ*, 814, 1, 53.
- Guzmán V. V. et al., 2017 *ApJ*, 836, 1, 30.
- Guzmán V. V. e., 2021 *in prep.*
- Hagemann R. et al., 1970 *Tellus*, 22, 6, 712.
- Harju J. et al., 2017 *ApJ*, 840, 2, 63.
- Hashiguchi M. et al., 2015 *Geochem. J.*, 49, 377.
- Hässig M. et al., 2017 *A&A*, 605, A50.
- Hayashi C. et al., 1985 *Protostars and Planets II* (D. C. Black and M. S. Matthews), pp. 1100–1153, UAP.
- Heays A. N. et al., 2014 *A&A*, 562, A61.
- Herbst E. and Klemperer W., 1973 *ApJ*, 185, 505.
- Herbst E. and van Dishoeck E. F., 2009 *ARA&A*, 47, 1, 427.
- Hesse R. and Harrison W. E., 1981 *Earth and Planetary Science Letters*, 55, 3, 453.

- Higuchi A. E. et al., 2019 *ApJL*, 885, 2, L39.
- Hily-Blant P. et al., 2017 *A&A*, 603, L6.
- Hily-Blant P. et al., 2019 *A&A*, 632, L12.
- Hily-Blant P. et al., 2020 *A&A*, 643, A76.
- Hincelin U. et al., 2011 *A&A*, 530, A61.
- Honvault P. et al., 2011 *PhRvL*, 107, 2, 023201.
- Horner J. et al., 2007 *Earth, Moon, and Planets*, 100, 1, 43.
- Hu R. et al., 2015 *Nature Communications*, 6, 10003.
- Huang J. et al., 2017 *ApJ*, 835, 2, 231.
- Hugo E. et al., 2009 *JChPh*, 130, 16, 164302.
- Hunten D. M., 1973 *Journal of Atmospheric Sciences*, 30, 8, 1481.
- Hunten D. M., 1982 *Planet. Space Sci.*, 30, 8, 773.
- Hunten D. M. et al., 1987 *Icarus*, 69, 3, 532.
- Iino T. et al., 2020 *The Astrophysical Journal*, 890, 2, 95.
- Iino T. et al., 2021 *The Planetary Science Journal*, 2, 4, 166.
- Inutsuka S.-i. et al., 2015 *A&A*, 580, A49.
- Isnard R. et al., 2019 *A&A*, 630, A27.
- Jakosky B. M. et al., 1994 *Icarus*, 111, 2, 271.
- Jennings D. E. et al., 2008 *The Astrophysical Journal*, 681, 2, L109.
- Jensen S. S. et al., 2019 *A&A*, 631, A25.
- Jensen S. S. et al., 2021 *A&A*, 650, A172.
- Jolly A. et al., 2010 *ApJ*, 714, 1, 852.
- Jørgensen J. K. et al., 2016 *A&A*, 595, A117.
- Jørgensen J. K. et al., 2018 *A&A*, 620, A170.
- Junk G. and Svec H. J., 1958 *Geochimica et Cosmochimica Acta*, 14, 3, 234.
- Kama M. et al., 2020 *A&A*, 634, A88.
- Kasting J. F. and Pollack J. B., 1983 *Icarus*, 53, 3, 479.
- Kastner J. H. et al., 2018 *ApJ*, 863, 1, 106.
- Kawabe R. et al., 1993 *ApJL*, 404, L63.
- Kissel J. and Krueger F. R., 1987 *Nature*, 326, 755.
- Kobayashi S. et al., 2003 *Geochem. J.*, 37, 663.
- Koerner D. W. et al., 1993 *Icarus*, 106, 1, 2.
- Kóspál Á. et al., 2013 *ApJ*, 776, 2, 77.
- Krijt S. et al., 2020 *ApJ*, 899, 2, 134.
- Krot A. N. et al., 2020 *Science Advances*, 6, 42, eaay2724.
- Kruijer T. S. et al., 2017 *Proceedings of the National Academy of Science*, 114, 6712.
- Lamberts T. et al., 2015 *MNRAS*, 448, 4, 3820.
- Lammer H. et al., 2018 *The Astronomy and Astrophysics Review*, 26, 1, 2.
- Lammer H. et al., 2020 *SSRv*, 216, 4, 74.
- Langer W. D. et al., 1984 *ApJ*, 277, 581.
- Lécluse C. and Robert F., 1994 *GeoCoA*, 58, 13, 2927.
- Lécuyer C. et al., 2017 *Icarus*, 285, 1.
- Lee J.-E. et al., 2008 *M&PS*, 43, 8, 1351.
- Lee J.-E. et al., 2019 *Nature Astronomy*, 3, 314.
- Lee M. R. et al., 2021a *Geochimica et Cosmochimica Acta*, 309, 31.
- Lee S. et al., 2021b *ApJ*, 908, 1, 82.
- Lellouch E. et al., 2001 *A&A*, 370, 610.
- Li C. et al., 2018 *ApJS*, 238, 1, 10.
- Liang M.-C. et al., 2007 *The Astrophysical Journal Letters*, 664, 2, L115.
- Lis D. C. et al., 2019 *A&A*, 625, L5.
- Liseau R. et al., 2012 *A&A*, 541, A73.
- Loison J.-C. et al., 2019a *MNRAS*, 484, 2, 2747.
- Loison J.-C. et al., 2019b *MNRAS*, 485, 4, 5777.
- Loison J.-C. et al., 2020 *MNRAS*, 498, 4, 4663.
- Loomis R. A. et al., 2020 *ApJ*, 893, 2, 101.
- Lupi A. et al., 2021 *A&A*, 654, L6.
- Lyons J. R. and Young E. D., 2005 *Nature*, 435, 7040, 317.
- Magalhães V. S. et al., 2018 *A&A*, 615, A52.
- Manfroid J. et al., 2009 *A&A*, 503, 2, 613.
- Marten A. et al., 2002 *Icarus*, 158, 2, 532.
- Martins Z. and Sephton M. A., 2009 *Extraterrestrial amino acids*, vol. 1 of *Amino acids, peptides and proteins in organic chemistry*, pp. 3–42, Wiley-VCH, Weinheim.
- Marty B., 2012 *Earth and Planetary Science Letters*, 313, 56.
- Marty B. et al., 2011 *Science*, 332, 6037, 1533.
- Mathews G. S. et al., 2013 *A&A*, 557, A132.
- McCanta M. C. et al., 2008 *Geochimica et Cosmochimica Acta*, 72, 23, 5757.
- McClure M. K. et al., 2016 *ApJ*, 831, 2, 167.
- McElroy M. B. and Hunten D. M., 1969 *J. Geophys. Res.*, 74, 7, 1720.
- McKeegan K. D. et al., 2006 *Science*, 314, 5806, 1724.
- McKeegan K. D. et al., 2011 *Science*, 332, 1528.
- Meier R. et al., 1998 *Science*, 279, 1707.
- Messenger S. et al., 2003 *Space Science Reviews*, 106, 155.
- Millar T. J. et al., 1989 *ApJ*, 340, 906.
- Miotello A. et al., 2014 *A&A*, 572, A96.
- Miotello A. et al., 2016 *A&A*, 594, A85.
- Mladenović M. and Roueff E., 2017 *A&A*, 605, A22.
- Mohapatra R. K. and Murty S. V. S., 2003 *M&PS*, 38, 2, 225.
- Molter E. M. et al., 2016 *The Astronomical Journal*, 152, 2, 42.
- Montmessin F. et al., 2005 *Journal of Geophysical Research (Planets)*, 110, E3, E03006.
- Moór A. et al., 2017 *ApJ*, 849, 2, 123.
- Mousis O. et al., 2002 *Icarus*, 159, 1, 156.
- Mumma M. J. and Charnley S. B., 2011 *ARA&A*, 49, 471.
- Nagaoka A. et al., 2005 *ApJL*, 624, 1, L29.
- Nakamura T. et al., 2008 *Science*, 321, 1664.
- Nakashima D. et al., 2012a *Meteoritics & Planetary Science*, 47, 2, 197.
- Nakashima D. et al., 2012b *Earth and Planetary Science Letters*, 357–358, 0, 355.
- Niemann H. B. et al., 2010 *Journal of Geophysical Research (Planets)*, 115, E12, E12006.
- Nixon C. A. et al., 2008a *ApJL*, 681, 2, L101.
- Nixon C. A. et al., 2008b *Icarus*, 195, 2, 778.
- Nixon C. A. et al., 2012 *The Astrophysical Journal*, 749, 2, 159.
- Noll K. S. et al., 1995 *The Astrophysical Journal*, 453, 1, L49.
- Nyman G. and Yu H.-G., 2019 *AIP Advances*, 9, 9, 095017.
- Oba Y. et al., 2014 *M&PS*, 49, 1, 117.
- Oba Y. et al., 2016 *MNRAS*, 462, 1, 689.
- Öberg K. I. et al., 2010 *ApJ*, 720, 1, 480.
- Öberg K. I. et al., 2011 *ApJ*, 734, 2, 98.
- Öberg K. I. et al., 2015 *ApJ*, 810, 2, 112.
- Öberg K. I. et al., 2021a *arXiv e-prints*, arXiv:2109.06268.
- Öberg K. I. et al., 2021b *AJ*, 161, 1, 38.
- Owen T. et al., 2001 *ApJL*, 553, 1, L77.
- Pagani L. et al., 1992 *A&A*, 258, 479.
- Pagani L. et al., 2003 *A&A*, 402, L77.
- Pagani L. et al., 2011 *ApJL*, 739, 2, L35.
- Paquette J. A. et al., 2021 *MNRAS*, 504, 4, 4940.
- Pepin R. O., 1991 *Icarus*, 92, 1, 2.
- Persson M. V. et al., 2014 *A&A*, 563, A74.
- Pester N. J. et al., 2018 *Geochimica et Cosmochimica Acta*, 242, 191.
- Piani L. and Marrocchi Y., 2018 *Earth and Planetary Science Letters*, 504, 64.
- Piani L. et al., 2015 *Earth and Planetary Science Letters*, 415, 0,

- 154.
- Piani L. et al., 2018 *Nature Astronomy*, 2, 317–323.
- Pierel J. D. R. et al., 2017 *AJ*, 154, 5, 178.
- Pineda J. et al., 2022 *Protostars and Planets VII*.
- Pinto J. P. et al., 1986 *Nature*, 319, 6052, 388.
- Podolak M. et al., 2002 *Icarus*, 160, 1, 208.
- Qi C. et al., 2008 *ApJ*, 681, 2, 1396.
- Qi C. et al., 2011 *ApJ*, 740, 2, 84.
- Ratajczak A. et al., 2009 *A&A*, 496, 2, L21.
- Redaelli E. et al., 2018 *A&A*, 617, A7.
- Richet P. et al., 1977 *Annual Review of Earth and Planetary Sciences*, 5, 65.
- Röllig M. and Ossenkopf V., 2013 *A&A*, 550, A56.
- Romano D. et al., 2019 *MNRAS*, 490, 2, 2838.
- Roueff E. et al., 2013 *Journal of Physical Chemistry A*, 117, 39, 9959.
- Roueff E. et al., 2015 *A&A*, 576, A99.
- Sakai N. et al., 2007 *ApJ*, 663, 2, 1174.
- Sakai N. et al., 2010 *A&A*, 512, A31.
- Sakamoto N. et al., 2007 *Science*, 317, 5835, 231.
- Salinas V. N. et al., 2017 *A&A*, 606, A125.
- Schmidt J. A. et al., 2013 *Proceedings of the National Academy of Science*, 110, 44, 17691.
- Schmitt-Kopplin P. et al., 2010 *Proceedings of the National Academy of Sciences*, 107, 7, 2763.
- Schramm L. et al., 1989 *Meteoritics*, 24, 99.
- Schroeder I. I. R. H. G. et al., 2019 *A&A*, 630, A29.
- Scott E. R. D. and Krot A. N., 2014 *Chondrites and their components*, vol. 1 of *Treatise on Geochemistry*, pp. 65–137, Elsevier, Oxford, second edn.
- Sebree J. A. et al., 2016 *Icarus*, 270, 421.
- Serigano J. et al., 2016 *The Astrophysical Journal*, 821, 1, L8.
- Shimajiri Y. et al., 2014 *A&A*, 564, A68.
- Shimizu K. et al., 2021 *Geochimica et Cosmochimica Acta*, 301, 230.
- Simkus D. N. et al., 2019 *Meteoritics & Planetary Science*, 54, 1, 142.
- Simon S. B. et al., 2007 *Geochimica et Cosmochimica Acta*, 71, 3098.
- Sipilä O. et al., 2017 *A&A*, 607, A26.
- Smith R. et al., 2009 *A&A*, 503, 265.
- Starkey N. A. and Franchi I. A., 2013 *Geochimica et Cosmochimica Acta*, 48, 0, 1800.
- Starkey N. A. et al., 2014 *Geochimica et Cosmochimica Acta*, 142, 0, 115.
- Stawikowski A. and Greenstein J. L., 1964 *ApJ*, 140, 1280.
- Sutton S. et al., 2017 *Geochimica et Cosmochimica Acta*, 211, 115.
- Takano S. et al., 1998 *A&A*, 329, 1156.
- Taniguchi K. et al., 2019 *ApJ*, 884, 2, 167.
- Taquet V. et al., 2012 *ApJL*, 748, 1, L3.
- Taquet V. et al., 2014 *ApJ*, 791, 1, 1.
- Teague R. et al., 2015 *A&A*, 574, A137.
- Telus M. et al., 2019 *Geochimica et Cosmochimica Acta*, 260, 275.
- Terzieva R. and Herbst E., 2000 *MNRAS*, 317, 3, 563.
- Thi W. F. et al., 2004 *A&A*, 425, 955.
- Thiemens M. H., 1999 *Science*, 283, 341.
- Thomas K. et al., 1993 *Geochimica et Cosmochimica Acta*, 57, 1551.
- Trapman L. et al., 2017 *A&A*, 605, A69.
- Tsuge M. et al., 2019 *ApJ*, 878, 1, 23.
- Tsuge M. et al., 2021 *ApJ*, 908, 2, 234.
- Tsukagoshi T. et al., 2019 *ApJL*, 878, 1, L8.
- Tsukamoto Y. et al., 2022 *Protostars and Planets VII*.
- Ueta H. et al., 2016 *PhRvL*, 116, 25, 253201.
- Vacher L. G. et al., 2017 *Geochimica et Cosmochimica Acta*, 213, 271.
- Vacher L. G. et al., 2020 *Geochimica et Cosmochimica Acta*, 281, 53.
- van der Marel N. et al., 2021 *A&A*, 651, L5.
- van Dishoeck E. F. et al., 2003 *A&A*, 400, L1.
- Villanueva G. L. et al., 2015 *Science*, 348, 6231, 218.
- Vinadier S. et al., 2007 *Icarus*, 191, 2, 712.
- Visser R. et al., 2009 *A&A*, 503, 2, 323.
- Visser R. et al., 2018 *A&A*, 615, A75.
- Vuitton V. et al., 2019 *Icarus*, 324, 120.
- Waite J. H. J. et al., 2009 *Nature*, 460, 7259, 1164.
- Walsh C. et al., 2015 *A&A*, 582, A88.
- Warren P., 2011 *Earth and Planetary Science Letters*, 311, 1–2, 93.
- Watanabe N. and Kouchi A., 2002 *ApJL*, 571, 2, L173.
- Watanabe N. and Kouchi A., 2008 *Progress In Surface Science*, 83, 439.
- Watanabe N. et al., 2010 *ApJL*, 714, 2, L233.
- Watson W. D., 1976 *Reviews of Modern Physics*, 48, 4, 513.
- Webster C. R. et al., 2013 *Science*, 341, 6143, 260.
- Willacy K. and Woods P. M., 2009 *ApJ*, 703, 1, 479.
- Williams J. P. and Best W. M. J., 2014 *ApJ*, 788, 1, 59.
- Wirström E. S. and Charnley S. B., 2018 *MNRAS*, 474, 3, 3720.
- Wirström E. S. et al., 2012 *ApJL*, 757, 1, L11.
- Wong M. H. et al., 2013 *Geophys. Res. Lett.*, 40, 23, 6033.
- Woods P. M. and Willacy K., 2009 *ApJ*, 693, 2, 1360.
- Wright I. P. et al., 1992 *GeoCoA*, 56, 2, 817.
- Yamagishi M. et al., 2019 *ApJ*, 875, 1, 62.
- Yamamoto D. et al., 2018 *The Astrophysical Journal*, 865, 2, 98.
- Yamamoto D. et al., 2020 *Meteoritics & Planetary Science*, 55, 6, 1281.
- Yan Y. T. et al., 2019 *ApJ*, 877, 2, 154.
- Yang L. et al., 2013 *Icarus*, 226, 256.
- Yurimoto H. and Kuramoto K., 2004 *Science*, 305, 5691, 1763.
- Yurimoto H. et al., 2008 *Reviews in Mineralogy and Geochemistry*, 68, 1, 141.
- Zhang J. S. et al., 2015 *The Astrophysical Journal Supplement Series*, 219, 2, 28.
- Zhang K. et al., 2017 *Nature Astronomy*, 1, 0130.
- Zhang K. et al., 2020 *ApJL*, 891, 1, L16.